Journal of Information Systems Engineering and Management
2025, 10(4)
e-ISSN: 2468-4376
https://www.jisem-journal.com/

Research Article

Optimized Design of Ductile Iron Valve Body Casting for Defect Minimization and Quality Enhancement

Vaibhav Maniar[1*], Pinank Patel[2]
[1*]Research Scholar in Department of Mechanical Engineering, Marwadi University, Rajkot-Morbi Road, Rajkot 360 003 Gujarat, India
E-mail: vrmaniar@gmail.com
[2]Associate Professor in Department of Mechanical Engineering, Marwadi University, Rajkot-Morbi Road, Rajkot 360 003 Gujarat, India
E-mail: Pinank.patel@marwadieducation.edu.in

ARTICLE INFO

Received: 12 Dec 2024

Revised: 23 Jan 2025

Accepted: 02 Feb 2025

ABSTRACT

Ensuring the production of superior castings devoid of foundry flaws while minimizing costs is a perpetual concern for foundries. Enhancing and refining manufacturing procedures are essential to attaining this objective. Computer simulation of foundry operations presents a contemporary substitute for costly and labour-intensive investigations in actual foundries, providing a reliable representation of casting. An in-depth investigation of the casting simulation outcomes enables the anticipation of several hazards that may lead to faults in castings, thereby diminishing their quality and, importantly, increasing production costs. This research analyses a computer simulation of ductile iron valve body casting at a Fine Cast Foundry. The valve body exhibited significant shrinkage defects, leading to a casting rejection rate of approximately 26%. A simulation of the casting process was conducted in accordance with actual shop-floor conditions. The initially designed gating and feeder system was found inadequate in mitigating the shrinkage issues. A revised configuration of the feeder system was proposed based on simulation insights, which, when implemented, led to a reduction in shrinkage-related defects from 26% to 1%. To ensure dimensional accuracy and realistic representation, 3D models were developed using NX 10.0 parametric software, and ProCAST was employed for casting simulation. Additionally, the Taguchi Design of Experiments (DOE) method was applied to optimize key green sand mould parameters. This statistical approach led to a significant reduction in sand mould-related defects, bringing the rejection rate down from 9% to 1.25%.

Keywords: *Ductile iron casting; valve body; simulation, gating design; design of experiment.*

1 Introduction

When it comes to numerically simulating the casting process, foundries rely heavily on physical and semi-empirical models. These models help simulate and study complex casting processes. These procedures may be modelled and solved with precision using simulation software that incorporates a numerical model. Simulation software and precise input data setup may improve operations and reduce trial-and-error in many foundries. Enhancing the gating design may reduce casting rejections and reduced the cost also.

Solidification simulation is a numerical modelling technique that assists in identifying thermal hotspots inside a mould. Flow simulation is essential for visualizing velocity of liquid ductile iron into the mould cavity, solidification of casting into the green sand mould and shrinkage prediction. It enables us to anticipate and mitigate melt flow disruptions, therefore forecasting the emergence of faults [1, 2]. Closed systems may have laminar or turbulent melt flow. Laminar flow continues until a certain velocity, when the flow of molten became turbulent. In turbulent places, liquid metal flows faster and pressure drops, which may entrain gas particles in the liquid iron casting. These elements erode the mould material, mimicking gaseous particles in the melt. These inclusions significantly impact cast component quality. The probability of particle entrainment increases with flow velocity, reaching 1.2 m/s, when mould damage is likely. Notches must have 0.5–1.0 m/s flow. [3-7]. Sand casting makes complicated metal sculptures in mass. The gating design help to fill liquid metal during casting. The riser system adjusts for cast material solidification shrinkage. [8, 9].

Journal of Information Systems Engineering and Management
2025, 10(4)
e-ISSN: 2468-4376
https://www.jisem-journal.com/

Research Article

Most casting and solidification problems result from incorrect gating system and feeder design and location. A well-designed gating system and intelligent casting location provide excellent mould cavity fills, controlled solidification, and feeding shrinkage.[10-12]. Taguchi's technique is popular in engineering product development. Simple changes in engineers' design methods may improve product quality. Taguchi organizes performance, quality, and cost optimization. Experiments are systematic ways to study a process. Changes to process inputs are tested and analysed to determine their effect on output. This experiment tries to uncover design factors that may be adjusted to improve noise resistance. [13-15] Shrinkage in the casting happens with negative solidification, especially when the melt is restricted inside the solidifying portion and the feeder solidifies before the casting. [16, 17].

Alongside the above-mentioned issues affecting casting quality, ductile iron shrinkage after solidification is important. Several writers discuss withdrawals and reasons. [18-20]. Shrinkage occurs between liquidus and solidus. Infusion may replace diminished volume to prevent them. Shrinkages and feeders are fully discussed in [21-24]. The feeder size depends on the casting volume capacity and cast alloy. To distribute metal throughout the casting during volumetric shrinkage, the feeder's form and size are vital to choosing the right feeder and placing it optimally. This procedure is heavily influenced by the gating mechanism and casting opening.[25, 26]. Due of its particular properties, this cast is ductile iron. Spherical graphite is in ductile iron's iron-carbon-silicon alloy matrix. The carbon concentration is 3.40%–3.90%. Carbon is high in thin-section casting. Graphite may float and degrade because to high CE and poor solidification rate (thick section). Thinner portions lower buoyancy. CE concentrations should exceed 4.2% (4.3–4.7%) in the thinner section. [27]. Melt cast iron, mostly grey and eutectic with few impurities, is altered to make spheroidal graphite. Pure magnesium or 5–10% magnesium alloys like Fe–Si–Mg are added to this procedure. Ready-to-cast iron needs 0.04 to 0.06% magnesium for graphite nodularity. Due to its lower melting temperature, castability, and machinability, ductile iron outperforms steel. The spherical graphite weakens the metal matrix little, causing minor notching. Mechanical qualities are similar to steels. Ductile iron's mechanical qualities depend on these phases' composition. Perlite is strong and rigid, whereas ferrite is tough and flexible. Alloying or heat treatment creates bainite, martensite, or austenite phases. This cast iron is susceptible to casting faults due to metallurgical processing quality. [28, 29].

Unavoidable physical phenomena like casting volume fluctuations following solidification cause shrinking. Technological intervention ensures casting shrinkage and solidification. [30]. Positively guided solidification and feeder placement are essential for a certain casting type, especially one with varied wall thickness [31, 32]. This study presents a novel, integrated approach to significantly reduce shrinkage and sand mould-related defects in ductile iron (SG iron) casting of valve bodies by combining advanced simulation, 3D modelling, and statistical design of experiments. The uniqueness of this research lies in:

- Systematic optimization of the gating and riser system using ProCAST casting simulation software, enabling visualization and elimination of shrinkage-prone zones before actual production.
- Use of NX software for precise 3D modelling, ensuring that geometric complexities of the valve body are accurately represented in the virtual environment.
- Application of the Taguchi Design of Experiment (DOE) method to systematically study and optimize green sand mould process parameters, leading to a significant reduction in sand-related defects.
- The integration of digital tools and experimental design methods into a cohesive workflow demonstrates an innovative, data-driven approach to traditional foundry challenges.

2 Material and Methods

Foundry faults, such as shrinkages, may affect brake disc castings, the final semi-finished product. Numerous completed studies and talks cover the vast subject. However, as it often involves a product, more research is needed. Computer simulation may be used for advanced study in many ways.

2.1 Material Overview:

EN-GJS-500-7, also known as SG Iron (Spheroidal Graphite Iron) or Ductile Iron grade 500-7, is a high-performance cast iron alloy characterized by a tensile strength of 500 MPa and an elongation of 7%. Its microstructure contains spherical graphite nodules, which impart excellent ductility, toughness, and impact resistance, making it highly suitable for critical components like valve bodies.

Advantages of SG Iron over other alternatives are shown in Table 1.

Journal of Information Systems Engineering and Management
2025, 10(4)
e-ISSN: 2468-4376
https://www.jisem-journal.com/

Research Article

Table 1 ***Comparison*** *of properties of SG Iron with other alternatives*

Material	**EN-GJS-500-7 (SG Iron)**	**Grey Cast Iron (e.g., EN-GJL-250)**	**Carbon Steel (e.g., ASTM A216 WCB)**	**Bronze/Brass Alloys**
Strength	High (500 MPa)	Moderate (~250 MPa)	High (~485–585 MPa)	Moderate
Ductility	Good (7%)	Poor (<1%)	Excellent	Good
Impact Resistance	Good	Poor	Excellent	Moderate
Cost	Moderate	Low	High	High
Corrosion Resistance	Moderate (can be enhanced)	Low	Moderate (depends on grade)	High
Machinability	Good	Excellent	Moderate	Good
Casting Complexity	Excellent	Excellent	Poor	Good

2.2 The chemical substances that make up EN-GJS-500-7

EN-GJS-500-7 ductile cast iron was selected for chemical analysis. A mobile spectrometer was used to analyse a pour sample before pouring. The element percentages are shown in Table 2

Table 2 Chemical make up of EN-GJS-500-7

Element	C	Si	Mn	S	P	Mg	Cu	Fe
%	3.58	2.70	0.20	0.01	0.01	0.05	0.11	93.34

Base melts were made in a 500 Kg medium frequency induction furnace at 250 Hz and 500 kW. The furnace crucible was charged with cast iron waste, silicon stamping, and foundry returns while 300kg of melt remained. The melt's chemical composition was changed by adding graphite and FeSi after melting. After heating to 1400 0C, 200 kg of the liquid alloy was transferred to a tundish ladle intended for magnesium treatment through a viable FeSiMg alloy utilizing cast iron scrap as covering.
After Mg-treatment, batches were carefully scraped and transported to a pouring equipment with pressured nitrogen and heating. Melt samples from the pouring basin during test part manufacture were analyzed to determine the chemical makeup of the Mg-treated alloys. Combustion was used to measure carbon and sulphur, while Spark Emission Spectroscopy measured the other elements. To fill two thermal analysis cups and record cooling curves, pouring basin samples were taken. Before the liquid alloy was added, one thermal analysis cup had the same composition as a commercial inoculant sample (size of grains 0.15–0.65 mm, 69.4 wt% Si, 4.1 wt% Al, 0.94 wt% Ca). The other cup was uninoculated.

2.3 Mechanical properties of EN-GJS-500-7

The mechanical properties of EN-GJS-500-7 is shown in Table 3.[33]
EN-GJS-500-7 is a spheroidal graphite iron that's commonly used in China and the United States. It's known for its good tensile strength and ductility, as well as its wear resistance and hardening capabilities.

Table 3 Mechanical properties of EN-GJS-500-7

Sr.No.	Mechanical Properties	Value	Unit
1.	Ultimate Tensile strength	500	$\frac{N}{mm^2}$
2.	Young modulus	169	$\frac{N}{mm^2}$
3.	Elongation	7	%
4.	Heat transfer coefficient	1000	W/m²/K

When shrinkage takes place in the casting, it compromises its integrity, potentially leading to failure under stress. Defects in the foundry—specifically, shrinkages that manifested during the casting process. The valve body experiences significant stress during operation, necessitating a minimal presence of internal defects in the casting which ultimately results in decline the mechanical properties.

Journal of Information Systems Engineering and Management
2025, 10(4)
e-ISSN: 2468-4376
https://www.jisem-journal.com/

Research Article

Two simulations were conducted to investigate and examine the casting. The previous assembly consisted of one feeder, whereas the new assembly consisted of three feeders.
The problem with this cast is that the surface seems to have shrunk. The X-ray showed this casting piece had reduced. Figure 1 shows a shrinking-faulted casting. Shrinkages result from insufficient metal depositing from the casting onto its surface during solidification.

Figure 1 Shrinkage defect in casting

2.4 Material used

The valve body castings are composed of ductile cast iron, complemented by a variety of other materials. These include new and parting sand, resin binders, catalysts, bentonite powder for facing sand, slag coagulant, pure aluminium, and asbestos. The materials employed in the casting process of the valve body are detailed in Table 4

Table 4 Materials used for casting

Sr. No.	Kind of material	Precise name	Amount	Unit
1.	CI	Ductile iron	300	Kg
2.	Green sand	Mixed sand	150	Kg
3.	Parting sand	Parting sand	1.5	Kg
4.	Metal additives	Magnesium	100	gm
5.	Sand binder	Bentonite	50	gm
6.	Impurity remover	De slagging agent	100	gm
7.	Furnace refractory	Aluminium oxide	10	Kg
8.	Scrap	Silicon stamping	10	Kg
9.	Foundry returns	Ductile iron gates, runners, risers	190	Kg

2.5 Data collection

Primary and secondary sources provided quantitative and qualitative data. This research collected data using several approaches. Identified methods:

An individual evaluation Practical survey questionnaire data was also acquired via critical observation in the manufacturing foundry's production zones. Direct observation occurred throughout casting. Possible manufacturing characteristics were identified during observation. Unintentional production variable changes by operators have been recorded. Conversations/dialogues A selected group inside the organization was interviewed. The interview/discussion included casting supervisors, casters, moulding operators, pattern fabricators, and the foundry quality control supervisor. The interview/discussion covered the company's product and process development plans and other quality challenges.
The data presented has been evaluated, and pertinent information has been extracted based on the specified requirements. The secondary data was gathered through an extensive review of various books, manuals, journals, websites, and by observing the operational sections of the company's foundry.

2.6 Cause effect diagram

Mould, metal, sand, shake out, and machine parameters are addressed in valve body casting. An Ishikawa diagram showed the valve body manufacturing characteristics that affect quality. Product designers and quality defect prevention use the Ishikawa diagram to identify possible elements that affect an outcome. Figure 2 shows

Journal of Information Systems Engineering and Management
2025, 10(4)
e-ISSN: 2468-4376
https://www.jisem-journal.com/

Research Article

the variation diagram for every defect cause. This figure helped identify process characteristics that affect valve body quality.

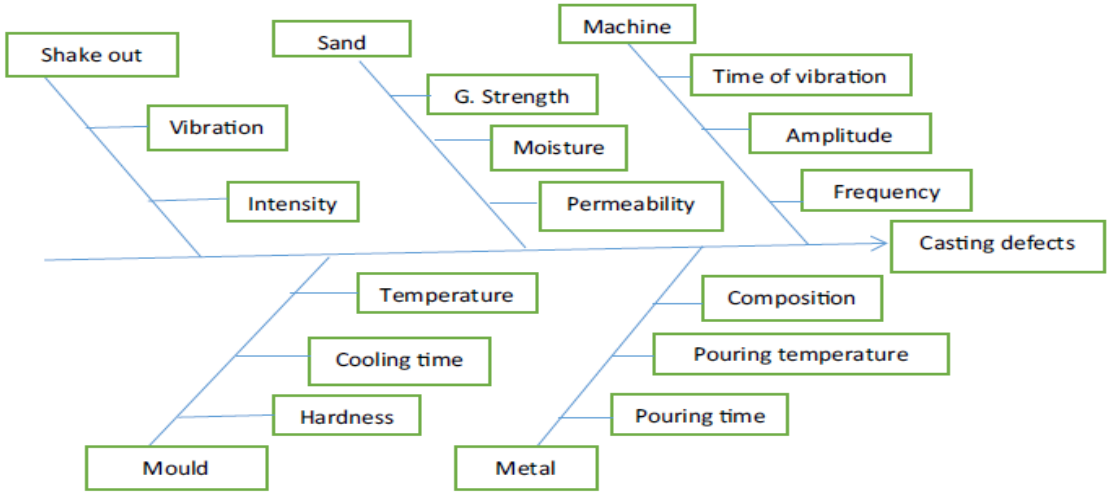

Figure 2 Cause effect diagram

2.7 Numerical experimentation

Quantitative testing the design of experiments approach, including the Taguchi method, may be used to discover ideal process parameters to minimize rejection rates owing to faults in new castings and valve body castings. A ishikawa diagram identified four process parameters—sand strength, AFS number, moisture content, and pouring temperature—to determine their effects on mould cavity filling and valve body casting form (

Table **5**). Three stages were selected for each process parameter to describe the investigational zone. These stages are based on accepted criteria and the foundry's valve body component casting expertise. Three settings—low level, medium level, and high level—have been chosen for each parameter. An orthogonal array selector determines the three factor and three level trials (

Table **5**). An orthogonal array, S/N ratio, and analysis of variance in Minitab 18.0 assess parameter impacts on answers.

Table 5 Process parameters along with set levels

Process parameters	**1-Low**	**2-Medium**	**3-High**
P: Moisture (%)	4.0	5.0	6.0
Q: Sand strength (Kg/m^2)	10000	12000	14000
R: AFS number	40	50	60
S: Pouring temperature ^{0}C	1300	1350	1400

The subsequent actions taken in the methodology involve the optimization of process parameters for sand casting of valve body castings through the application of the Taguchi method.

2.8 CAD model of casting

Three-dimensional representation of a valve body Modelling has been conducted utilizing SolidWorks (CAD) software. The 3D geometry of the valve body, along with the gating system, is illustrated in Figure 3 using SolidWorks. Ductile iron is used for the valve body, which has a 280-mm outside diameter, 140-mm inner diameter, and 45-mm height. The sand mould and castings are modelled with proportionate proportions. The 3D CAD model was created in SolidWorks for valve body casting. All components were then placed in their mould places.

Journal of Information Systems Engineering and Management
2025, 10(4)
e-ISSN: 2468-4376
https://www.jisem-journal.com/

Research Article

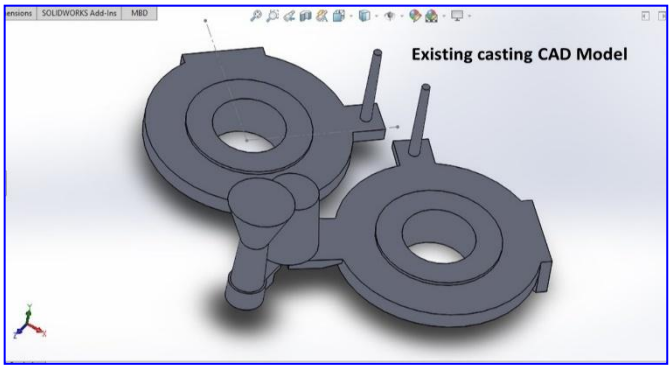

Figure 3 Existing CAD model of casting

Casting process simulation includes using mathematical equations in a computer software to replicate a genuine phenomenon. The simulation applications leverage finite element analysis of three-dimensional casting models and enhanced user interface, calculation, and visualization capabilities. The casting model, including feeders and gates, must be created in SolidWorks and loaded into ProCAST. A finite element method-based algorithm or software has been used to analyse mould filling and solidification in casting simulation to discover faults including shrinkage porosities, air entrapment, and misrun. ProCAST program developed the valve body mould 3D model of existing casting in Figure 4.

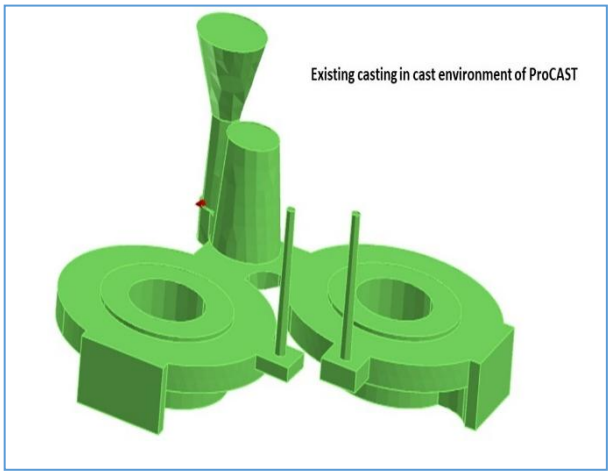

Figure 4 Existing CAD model in ProCAST environment

2.9 Tools and equipment utilized for moulding

Table 6,and

Table 7 list the valve body casting tools and equipment used for mould creation and completion:

Table 6 Hand tools used in casting

Sr. No.	Name of hand tool	Application
1.	Slick	Smoothing and repairing surfaces of the mould cavity to maintain precise dimensions.
2.	Gate cutter	Cutting gates, sprues, or risers in the mould for proper metal flow and solidification.
3.	Lifters	Removing unwanted sand from deep or narrow mould sections.
4.	Sprue cutter	Cutting sprue holes in the mould to facilitate the flow of molten metal.
5.	Wire brush	Cleaning and removing loose sand or other residues from moulds or cores before pouring.
6.	Shovel	Handling and transporting moulding sand to the working area.
7.	Meter	Measuring dimensions of valve body casting

Journal of Information Systems Engineering and Management
2025, 10(4)
e-ISSN: 2468-4376
https://www.jisem-journal.com/

Research Article

8.	Mobil	For indication of room temperature during valve body casting

Table 7 Moulding equipment and testing machines used

Sr. No.	Equipment	Application
1.	Moulding box	Prepare the mould for casting of valve body
2.	Tundish ladle	Holding molten metal and for de sulphurising liquid metal for pouring
3.	Sieve analyser	To obtain AFS number
4.	Thermocouple	To measure temperature of molten metal in furnace
5.	Induction furnace	To melt 500 kg charge of ductile iron casting based on electromagnetic induction principle
6.	Deep pocket mould hardness tester	To measure mould hardness
7.	Digital moisture tester	To measure moisture content in moulding sand
8.	Universal sand strength testing machine	To measure strength of moulding sand
9.	Digital permeability testing machine	To measure permeability of moulding sand

3Analysis of data

3.1 Analysis of empirical observations and interviews

The data collected through the aforementioned methods have undergone both quantitative and qualitative analysis. The analysis of the data employs a range of tools provided by Minitab 18 software. Sand casting flaws have been lessened based on the results of the data analysis.

Experts in pattern, moulding, and melting were interviewed to assess valve body casting process parameters and identify problem reasons. Interviews and conversations indicated that equipment problems, process variances, insufficient sand characteristics, malfunctioning gating systems, labour concerns, and inappropriate valve body casting techniques might cause errors.

The components involved in valve body castings are analysed to identify the casting defects that arise during the casting process. The existing sand properties are shown in Table 8

Table 8 existing sand properties

Property	**Typical/Standard Value**	**Existing Tested Value**	**Test Method / Standard**	**Testing Description**
Grain Fineness Number (GFN)	55 – 85 AFS	50	AFS 1114-87-S	Sand is sieved through a stack of standard screens; average grain size is calculated.
Permeability Number	80 – 120	78	AFS 5222-13-S	Measures airflow through a standard sand specimen using a permeability meter.
Green Compressive Strength	30 – 80 kPa (4.5 – 11.5 psi)	25	AFS 3311-00-S	Compression applied to a cylindrical sand specimen until failure.
Green Shear Strength	15 – 40 kPa (2.2 – 5.8 psi)	13.5	AFS 3312-00-S	Shear force is applied using a sand strength tester until rupture.
Moisture Content	2.5% – 4.0%	1.5%	AFS 2211-00-S	Determined by drying a known mass of sand and measuring weight loss.
Mold Hardness	70 – 85 (B scale)	80	AFS 3323-00-S or Portable Hardness Tester (Dial type)	Measures resistance of mold surface to penetration.

Journal of Information Systems Engineering and Management
2025, 10(4)
e-ISSN: 2468-4376
https://www.jisem-journal.com/

Research Article

3.2 Production of valve body

The valve body was produced with great regard to design criteria for material and casting tolerances. Design requirements for the valve body include a 9.6 kg net weight, Ø280 mm OD, Ø140 mm ID, and 45 mm height. SolidWorks software was used to create the valve body's 3D model according to the specifications. Figure 5 illustrates the geometry of the valve body.

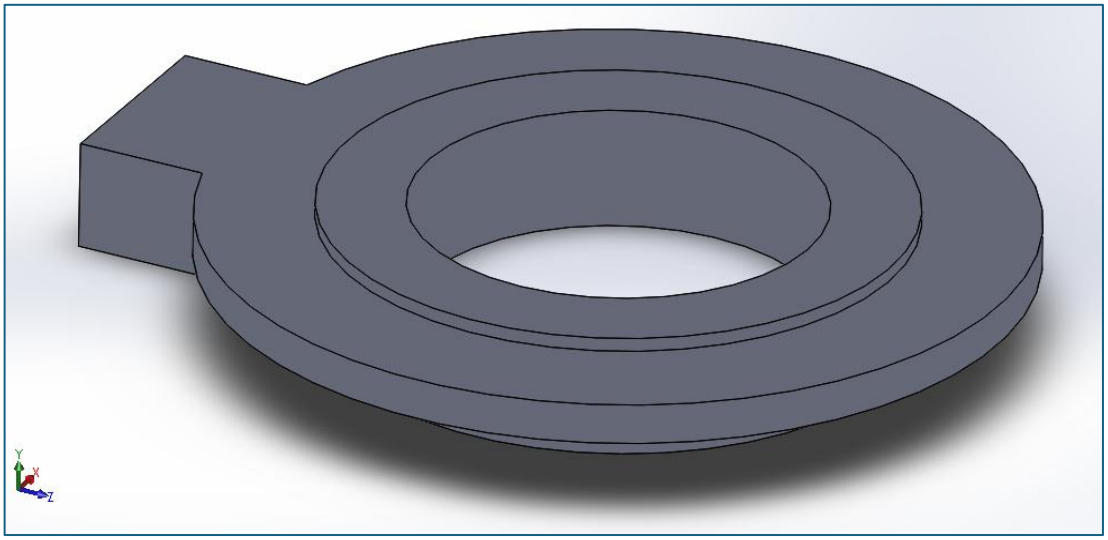

Figure 5 Valve body model

3.2.1 Specification for pattern design

For valve body fabrication, the foundry produced a template that accounts for machining, shrinkage, and draft angle. A wooden pattern with a diameter of Ø280mm and height of 45mm has been created in the pattern section. SolidWorks software was used to create the pattern's 3D geometry according to starting specifications. Here machining allowance was kept 2mm, shrinkage allowance was 2 % and draft angle was set at 2 degrees.

3.2.2 Moulding box selection for green sand mould

The valve body's bulk weight comes from molten metal injected into the mould chamber. This procedure selects a flask based on pattern dimensions and cavity end clearances.

The casting weighs 25–30 kg. Minimum clearances are 75 mm on each side for mould height, 300 mm for breadth, and 350 mm for flask length. Thus, the minimum flask length for mould preparation is 1500 mm, based on the pattern diameter, side clearances, ingate length, and riser diameter. As shown in Figure 6 Moulding box geometry, a flask that matches these values was selected. Six flasks were used to build the mould. Single flask measurements for valve body castings are shown in Figure 6. Each side of the moulding box set to 1500 mm, and thickness of wall to 10 mm.

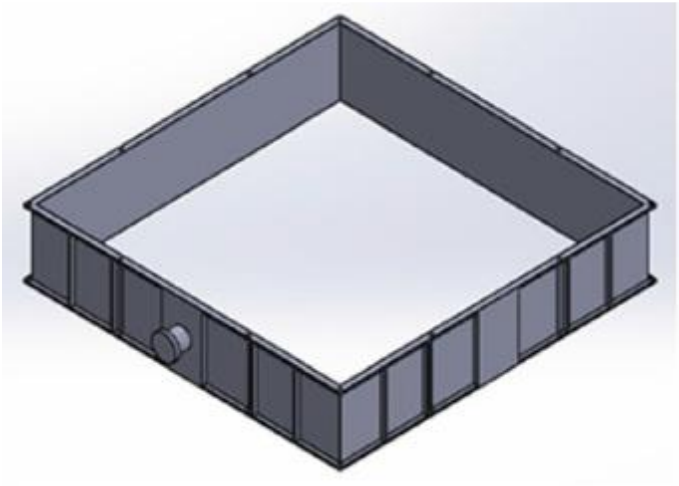

Journal of Information Systems Engineering and Management
2025, 10(4)
e-ISSN: 2468-4376
https://www.jisem-journal.com/

Research Article

Figure 6 Moulding box geometry

3.2.3 Analysis of clay content in mould sand

Moulding sand clay particles may not settle in water after a certain period. Particles are usually < 20 microns wide. The examination of clay content includes all very fine clay content. [34, 35]. Mould-making silica sand has been tested for clay content for each valve body casting sample.

Error! Reference source not found. displays the proportion of each sample test's result using Equation (1).

$$Clay\ content\ (\%) = \frac{(\omega_{sb})-(\omega_{sa})}{\omega_{sb}} * 100 \quad \ldots (1)$$

ω_{sb} denotes the mass of sand prior to wash, whereas ω_{sa} represents the mass of sand subsequent to wash. The percentage of clay for sample one was assessed and recorded as follows:

$$Clay\ content\ (\%) = \frac{100 - 92.50}{100} * 100 = 7.50$$

In a similar manner, the results for samples two, three, four, and five were found to be 6.8, 7.36, 6.44, and 8.34, separately.

The average clay of the green sand utilized for valve body casting has been specified based on the five samples presented in Table 9. The calculation is straightforward: it involves summing all the clay fractions and dividing by the total number of specimens, resulting in a value of 7.29%. The findings indicate that this is acceptable, with the muddy effect of sand being minimal.

Table 9 The moulding sand utilized contains clay content.

Sample	the mass of sand prior to wash in grams	represents the mass of sand subsequent to wash in grams	Clay %
1.	100	92.50	7.5
2.	100	93.20	6.8
3.	100	92.64	7.36
4.	100	93.56	6.44
5.	100	91.66	8.34

3.2.4 Analysis of sand using AFS

The Average fineness number (AFS) measures average grain sizes based on sieve analysis. Sand grains are tightly packed in moulds made of exceptionally fine-grained sands. Porosity flaws result from air and gas entrapment due to space constraints. Coarse sands might cause unnecessary casting flaws. To make good castings, the AFS values of moulding sand have to be in a certain range. AFS is calculated as the sum of the multiplication numbers for each retained riddle (percentage retained and multiplied by this number-a constant specific to that sieve). A sample of the moulding sand is weighed for the AFS number, according to Eq. (2) [36].

$$AFS = \frac{sum\ of\ all\ products}{total\ percentages\ gathered\ in\ shieve} = \frac{\Sigma R_i M_i}{\Sigma R_i} \quad \ldots (2)$$

Here, M_i represents multiplication factor for i^{th} riddle, R_i denotes the quantity of sand cleave to the i^{th} riddle.

AFS of the used sand for the valve body casting is given in
Table ***10***.

The AFS of the green sand found to be 46.92. This result is categorized as very fine sand, which caused porosity in the valve body casting because the mould was compressible from this type of sand.

Table 10 GFN outcomes of blended sand used in valve body casting

sr.no	sieve size in microns	weight of sieve without sand in grams	weight of sieve with sand in grams	retained sand weight in grams	% of retained sand (R_i)	Multiplier factor (M_i)	Product of (R_i X M_i)
1	1700	318	319.53	1.53	1.53	5	7.65
2	850	289	289.93	0.93	0.93	10	9.3
3	600	305.5	312.17	6.67	6.67	20	133.4
4	425	288	311.43	23.43	23.43	30	702.9
5	300	257	276.29	19.29	19.29	40	771.6
6	212	294.5	322.44	27.94	27.94	50	1397
7	150	261	275.35	14.35	14.35	70	1004.5

Journal of Information Systems Engineering and Management
2025, 10(4)
e-ISSN: 2468-4376
https://www.jisem-journal.com/

Research Article

8	106	246	249.85	3.85	3.85	100	385
9	75	255.5	257.01	1.51	1.51	120	181.2
10	53	252	252.5	0.5	0.5	200	100
11	Span	267	267	0	0	300	0
Total		100		Total		4692.55	

3.2.5 Assessment of casting total mass

A casting's gross mass is the mass of the liquid or molten metal in the mould cavity including all gating system components. This comprises the valve body pattern casting's net mass and any material removed during fatling such as risers, riser bases, sprues, pouring cups, and ingates. The highest ductile iron cast yield for this task is 90%. Casting gross mass was calculated using Eq. (3) [37].

$$Gtoss\ mass\ of\ casting = \frac{Net\ mass\ of\ vavle\ body\ casting}{maximum\ yield\ of\ ductile\ iron\ casting} \quad \ldots (3)$$

$$\omega_g = \frac{9.6}{0.9} = 10.67\ Kg$$

Where, ω_g is gross mass of casting in Kg.

This mass is regarded as beneficial for achieving the target valve body weight of 9.0 kg, as well as for filling the cavities of the gating system involved in the casting development.

3.2.6 Improving and integrating metallic additions into ductile iron casting

The process of melting ductile solid metal was traditionally carried out in a furnace. However, the degassing operation, which involves the removal of oxygen gas from the molten ductile cast metal, is achieved by introducing clean aluminium into the molten material within the furnace. This is done prior to transferring the metal into a preheated tundish ladle before pouring.

The addition of pure aluminium is thought to interact with the existing O_2 or form CO_2 bubbles and escape outside the molten metal. Consequently, carbon levels should be reduced to the desired extent following deoxidation, which mitigates the detrimental effects of elevated oxygen content in the melt, thereby enhancing durability.

3.2.7 Assessment of pouring duration

The duration required to pour liquid ductile iron into the mould for casting valve body has been established and contrasted with the definite mould filling interval recorded during the pouring process. The fluidity constant of ductile iron (f) is 0.6 and the pouring temperature of ductile iron is 1350 °C, to ascertain the filling time. Consequently, the duration for pouring ductile iron with a mass not exceeding 450 kg has been determined using the experiential equation presented in Equation (4), as follows:

$$t_p = f\left(1.24 + \frac{S}{16.65}\right)\sqrt[3]{\omega_g} \quad \ldots(4)$$

Where t_p is pouring time in seconds, S is average casting thickness, ω_g is gross weight of casting.

$$t_p = 0.6\left(1.24 + \frac{95}{16.65}\right)\sqrt[3]{10.67} = 9\ seconds$$

The minimum time required for the ductile iron casting mass of 10.67 kg to fully fill the entire mould cavity.

3.2.8 Development of gating system

The gating mechanism helps fill the mould chamber with molten metal during casting. The feeders replace melt lost during metal solidification and shrinkage, making them essential to the gating system. Shrinkage reduces size via linear and volumetric changes.

The valve body is cast using the gating technique with a longitudinal slice "S_A" at the bottom sprue, as shown in Figure 7

The defining longitudinal slice S_A is located at the bottommost of the sprue, unlike vacuum gating system's ingate location, following a conventional ratio of 1:1.2:1.4 [21, 38].

The calculation of S_A is performed as outlined in Equation (5):

$$S_A = \frac{22.6\omega_g}{\rho F t_p \sqrt{H}}\ [cm^2] \quad \ldots (5)$$

Where ρ is density in g/cm^3, F is friction factor, t_p is pouring time in seconds, H is effective pouring height in cm.

Journal of Information Systems Engineering and Management
2025, 10(4)
e-ISSN: 2468-4376
https://www.jisem-journal.com/

Research Article

$$S_A = \frac{22.6 * 10.67}{7.1 * 0.31 * 9\sqrt{5.88}} [cm^2] = 5\ cm^2$$

The predicted S_A determining cross-section was 5 cm². The estimated determining cross-section is used to determine the cross-sections of other gating system components. Calculations for gating system components were done using the ratio:
Runner cross sectional area $1.2 \times S_A$ = 6 cm²and sprue cross sectional area as $1.2 \times 1.2 \times S_A$ = 7.2 cm².
Figure 7 shows the original gating system, feeders, and casting assembly. Three feeds are used in the top casting portion.

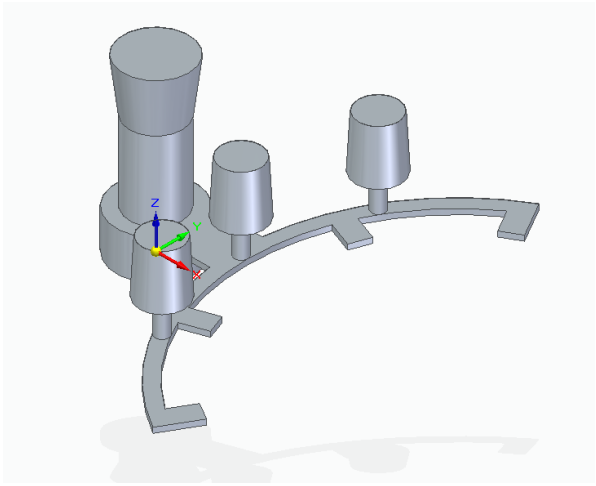

Figure 7 Proposed feeders and gating system

3.2.9 Sprue Design

It is generally tapered downward to minimize air aspiration during sand casting. It guides molten metal to the ingate without turbulence, enabling it to enter the mould cavity. [39].
Based on diameter of sprue at exit (D_e) from S_A can be determined as follows equation (6) was 2.5 cm. The diameter of the upper sprue is 1.15 times that of the outlet sprue; hence, it has been shown that the inlet sprue diameter (D_i) is 2.7 cm.

$$S_A = \frac{\pi D_e^2}{4}$$

The height of valve body casting is 45mm, and accordingly, the length of sprues can be arranged to that distance. The present sizes of all sprues prepared with 25mm at upper end, 30 mm at lower end, and height of 25mm fit the designed plans as shown in Figure 8. The predicted entry and outlet areas of the sprue are 707 mm² and 491mm², respectively.

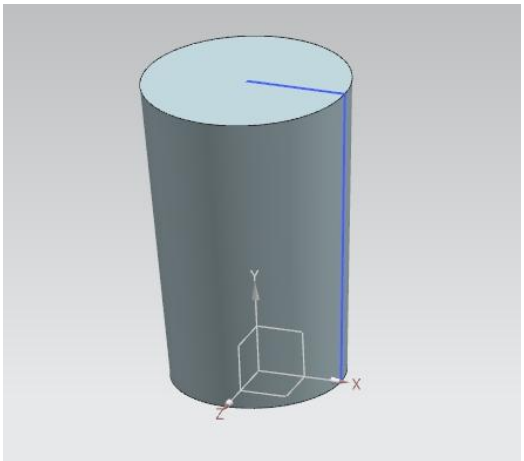

Figure 8 CAD Model of sprue

The sprue has a frustum-like shape, and frustum Equation (6) was used to calculate the metal volume within.

Journal of Information Systems Engineering and Management
2025, 10(4)
e-ISSN: 2468-4376
https://www.jisem-journal.com/

Research Article

$$volume\ of\ sprue = \frac{1}{2}\pi h(D_e^2 + D_i^2 + D_e D_i) \ \ldots (6)$$

$$volume\ of\ sprue = \frac{1}{2} * \pi * 4.5(2.5^2 + 3^2 + 2.5 * 3)$$
$$= 160.81\ cm^3$$
$$V_{sprue} = 160.81\ cm^3$$

The mass of sprue was determined by means of Equation (7) and material density of 7200 kg/m³.

$$mass\ of\ sprue = volume\ of\ sprue * density\ of\ material \ldots (7)$$
$$Mass\ of\ sprue = \ 1.15\ Kg$$

3.2.10 The sprue base well

It holds metal at the bottom of the sprue, thus slowing down metal flow and preventing mould erosion. The pattern for the sprue base is a ductile iron valve body casting of diameter (d) 30 mm and height (h) 40 mm in constructing the cavity. Figure 9 depicts the geometry of the sprue base.

$$volume\ of\ hot\ well = \frac{\pi}{4}d^2h = \frac{\pi}{4} * 30^2 * 40 = 28.27 * 10\text{^}3\ mm^3$$

Equation (7) was used to compute the metal mass in the sprue base to 0.2 kg. It has effectively pressed the ingate metal. The sprue base cavity casting yield meets valve body casting weight requirements.

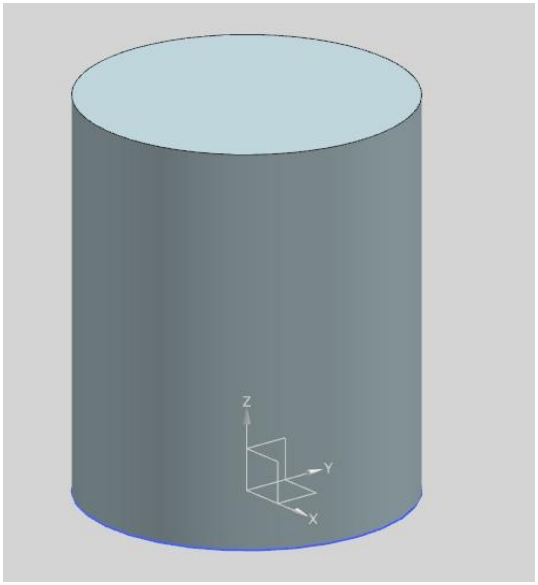

Figure 9 CAD model of hot well

3.2.11 Development of a pouring basin

The pouring basin first directs liquid ductile iron into the sprue. A pouring basin has a 4cm entrance, 3cm exit, and 3cm height. Pouring basin arrangement is seen in Figure 10.

Journal of Information Systems Engineering and Management
2025, 10(4)
e-ISSN: 2468-4376
https://www.jisem-journal.com/

Research Article

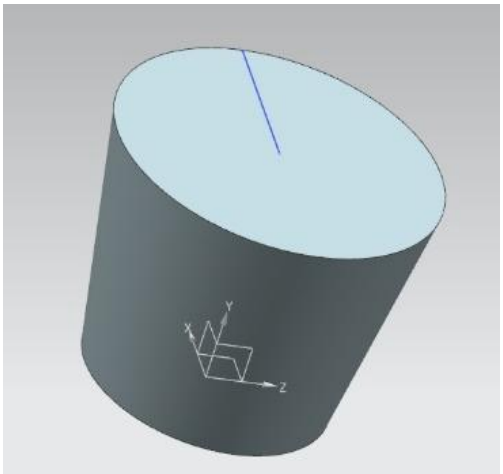

Figure 10 CAD model of pouring basin

$$volume\ of\ pouring\ basin = \frac{1}{2}\pi h_b(P_e^2 + P_i^2 + P_eP_i)$$

Where, P_e is exit diameter of pouring basin, P_i is inlet diameter of pouring basin and h_b is height of pouring basin.

$$volume\ of\ pouring\ basin = \frac{1}{2}\pi * 3(3^2 + 4^2 + 3 * 4) = 174.35\ cm^3$$

The liquid ductile iron volume in the pouring basin is calculated to be 174.35 cm^3. Equation (7) calculates 1.25 kg for the liquid ductile iron in the pouring cup. The casting yield at the gating system pouring basin pressured sprue cavity, but it also eroded sand. This reduced and closed the sprue departure region, solidifying metal in the gating design

3.2.12 Chock area design

The main control zone controls metal flow into the mould void to fill it within t pouring time. Chock area was calculated using Equation (8).

$C_A = \frac{\omega_g}{\rho * t_p * \epsilon * \sqrt{2 * g * S_H}}$ ... (8)

Where, C_A is chock area, ω_g is mass of casting in Kg, ρ is mass density of ductile iron in Kg/mm^3, ϵ is efficiency factor considered here is 0.75, S_H is height of sprue in mm.

$$C_A = \frac{10.67}{7.2 * 10^{-6} * 9 * 0.75 * \sqrt{2 * 9810 * 40}} = 209\ mm^2$$

The chock area as calculated is 209 mm^2, resulting in a chock diameter of 16.31 mm. Hence design value is taken as 17 mm.

3.2.13 Riser design

Risers eliminate porosities by addressing casting shrinkage during solidification. A feeder or riser stores liquid metal and supplies it to castings that need it. Liquid metal rise up in the mould after filling mould cavity. Liquid ductile iron in the riser prevents shrinkage flaws in the final product during casting solidification. [40]

The valve body casting riser has been tested to verify it meets Chvorinov's regulation criteria. To avoid shrinkage contraction when the molten metal cools during solidification, it must have enough metal. Equation (9) determines riser or casting solidification time.

$Solidification\ time, T_S = K * \left[\frac{volume\ of\ riser}{surface\ area\ of\ riser}\right]^2$ ... (9)

K represents a constant that encapsulates the characteristics of mould material. The solidification state in the valve body casting development illustrated in the equation (10) [41].

$T_S(riser) > T_S(casting)$ ... (10)

Current design of riser:

Let d_r= diameter of cylindrical riser=10 mm
And h_r= height of cylindrical riser = 50mm

Journal of Information Systems Engineering and Management
2025, 10(4)
e-ISSN: 2468-4376
https://www.jisem-journal.com/

Research Article

A_r =Surface are of cylindrical riser = $\left(\pi d_r h_r + 2\ \frac{\pi}{4}\ {d_r}^2\right)$=1727.87 mm²

V_r =Volume of cylindrical riser =$\left(\frac{\pi}{4}\ {d_r}^2 h_r\right)$ = 3927 mm³

Ration of surface are of cylindrical riser to its volume is

$$\frac{A_r}{V_r} = 0.44\ mm^{-1}$$

Mass properties obtained from solid cast 3-D Model as follows

Surface Area of casting A_C=157184.85 mm²

Volume of Casting V_C= 1344679.31 mm³

$\frac{A_C}{V_C}$ =0.166 mm^{-1}

From above equations $\frac{A_r}{V_r} > \frac{A_c}{V_c}$, The riser solidified first, which is not ideal for achieving sound casting and may result in shrinkage defects.

Proposed riser design

The volumetric shrinkage of ductile iron is currently observed to be 0.1%. [21]

So required volume of riser (V_r) is

$V_r = 3 * \ volumatric\ shrinkage\ of\ ductile\ iron\ casting * volume\ of\ casting$

$$V_r = 3 * \ 0.1 * \ 1344679.309 = 403404\ mm^3$$

Now design of riser is at ration of surface area to volume of riser to be minimum,

$$\frac{\partial A}{\partial d} = 0$$

$$\frac{\partial}{\partial d}\left(\pi d_r h_r + 2\ \frac{\pi}{4}\ {d_r}^2\right) = 0$$

we have $(h_r) = \frac{4V_r}{\pi {d_r}^2}$

Substituting above value of h_r,

$$\frac{\partial}{\partial d}\left(\pi d_r \frac{4V_r}{\pi d^2} + 2\ \frac{\pi}{4}\ {d_r}^2\right) = 0$$

$$\frac{\partial}{\partial d}\left(\frac{4V_r}{d} + 2\ \frac{\pi}{4}\ {d_r}^2\right) = 0$$

$$\left(-\frac{4V_r}{d^2} + \pi\ d_r\right) = 0$$

$$Thus, V_r = \frac{\pi}{4}\ {d_r}^3$$

But we have, $V_r = \frac{\pi}{4}\ {d_r}^2\ h_r$

From above Equation d_r=$h_r$for cylindrical riser, and d_r=h_r=80 mm,

So Proposed diameter and height of cylindrical riser is 80 mm which satisfy following criteria, hence we had taken combination of diameter and height as 50 mm and 205 mm respectively for the riser.

$$\frac{A_r}{V_r} \leq \frac{A_c}{V_c}$$

3.2.14 Assessment of the freezing ratio between casting and riser

To avoid valve body solidification shrinkage or macro porosity, the riser's solidification time has been compared to the valve body casting's freezing ratio. The modulus technique was used to compute the riser's freezing ratio (FR) to the casting using Equation (21) [20].

$$F_R = \frac{\left(\frac{volume}{surface\ area}\right)_{riser}}{\left(\frac{volume}{surface\ area}\right)_{casting}} \qquad \ldots (11)$$

$$F_R = 1.356$$

This approach indicates that the volume to area (V/A) ratio of the riser is 11.6, in contrast to the casting V/A ratio of 8.55, meaning the riser V/A is 1.356 times that of the casting.

Consequently, the riser freezing duration significantly exceeds the casting freezing duration and the valve body castings produced are of high quality.

Journal of Information Systems Engineering and Management
2025, 10(4)
e-ISSN: 2468-4376
https://www.jisem-journal.com/

Research Article

3.2.15 Assessment of pouring velocity

The maximum velocity of the molten metal can be calculated using Equation (12)

$P_V = \sqrt{2gP_H}$ ... (12)

Where, P_V is pouring speed in m/sec, and P_H is pouring head in meter.

Consequently, the speed of the metal at the base of the pouring basin (near the entrance of the sprue from the two heads)

$$P_{0.75} = \sqrt{2 * 9.81 * (0.8 + 0.03)} = 4.03\ m/s$$

And

$$P_{0.45} = \sqrt{2 * 9.81 * (0.45 + 0.03)} = 3.06\ m/s$$

Where 0.03 added to head term is height of pouring basin in m.

The first velocity is supposed to occur briefly, but the succeeding velocity persists until the pouring is complete. The sprue lip erosion may create initial velocity. Thus, this research analyses metal fluxes in valve body casting channels at 3.06 m/s.

Eq. (13), which accounts for the sprue wall's surface friction coefficient (FC), determines the metal's maximum critical velocity at the bottom or exit.

$CV_{VMAX} = F_C\sqrt{2gS_h}$ ... (13)

Where, where CV_{VMAX} represents the maximum pouring velocity in m/s and S_H denotes the sprue height in meters, which is 0.04 meters. So,

$$S_{\ p,exit} = 0.2 * \sqrt{2 * 9.81 * 0.04} = 0.18\ m/s$$

Consequently, the Reynolds numbers are 64480 at the sprue inlet and 48960 at the outlet.[42]

3.2.16 Assessment of riser solidification duration

Equation (14) calculates the time required to freeze a riser for ductile iron valve body casting. Riser and casting materials are same.

$R_{ST} = \left[\frac{\pi}{4}\left(\frac{\rho_L \Delta H_L}{T_M - T_i}\right)^2 \left(\frac{1}{\rho_G K_G C_G}\right)\right]\left[\frac{V_{SO}}{A}\right]^2$ ... (14)

R_{ST} is the riser solidification time. The numbers ρ_G, K_G, and C_G represent the density, specific heat, and thermal conductivity of green sand mould material, according to standard. H_L represents latent heat of solidification, whereas ρ_L represents liquid metal casting density, both taken from standard tables. V_{SO} is the solidified riser volume, A is its interface area, T_M is the melting point temperature in degrees Celsius, and Ti is the mould wall's starting temperature in degrees Celsius. This scenario assumes constant characteristics throughout casting. Total solidification time, R_{ST} = 48.23 = 2 days. The riser cemented following casting solidification, indicating that the design is suitable for sound valve body casting.

3.2.17 Assessment of the mean flow rate

In Equation (15), the total mass of the casting divided by real filling time yields the valve body's average molten metal flow rate. [43].

$F_R = \frac{\omega_g}{T_P}$ ... (15)

Where, A_{FR} is mean flow rate in Kg/sec, ω_g is gross mass of casting, in Kg and T_P is pouring time in seconds,

$$A_{FR} = \frac{10.67}{9} = 1.185\ kg/s$$

Mould channel cavities are expected to receive 1.185 kg per second of metal mass from the gating system cavities. Equation (16) determines valve body mould cavity filling time (M_{FT}). [44].

$M_{FT} = \frac{volume\ of\ mould\ cavity}{flow\ rate} = \frac{V_M}{Q}$ ... (16)

V_M is the valve body mould cavity capacity (0.0014 m^3), whereas Q is the metal flow rate (0.000127 m^3/s) based on velocity and cross-sectional area at the sprue bottom.

$$M_{FT} = \frac{0.0014\ \text{m}^3}{0.000127\ \text{m}^3/\text{s}} = 11.0\ sec$$

3.2.18 Assessment of thermal loss to the gating system

To avoid misruns and penetration faults, the ductile iron was melted and poured at the right temperature. Pouring temperature at furnace is 1350 °C (from tundish ladle to mould sprue entry). However, heat dissipation in the gating system prevent the liquid iron from reaching the mould cavity at this pouring temperature. When liquid metal is poured into the gating system, the temperature drops. Therefore, diminished fluidity caused

Journal of Information Systems Engineering and Management
2025, 10(4)
e-ISSN: 2468-4376
https://www.jisem-journal.com/

Research Article

casting product misrun or penetration flaws. The temperature loss of molten ductile iron in the gating system was computed by Eq. (17). [46].

$$T_L = \frac{SA_{INGATE}(T_P - T_i)\sqrt{t_p}}{\omega_g C_L} * \sqrt{\sigma_G K_G C_G} \quad \ldots (17)$$

SA_{INGATE} indicates the combined surface area of all ingate systems in m², TP indicates pouring temperature (°C), Ti indicates starting temperature (°C), tp indicates pouring duration (in seconds), and ω_g indicates casting and gating system mass (kg). C_L represents the specific heat of liquid metal, measured in J/kg × °C, as per standard tables. Mould material thermal conductivity (K_G) is measured in J/s·m·°C, whereas density (σ_G) is reported in kg/cm³. C_G is the J/Kg × °C specific heat of the mould material, given as $\sigma_G K_G C_G$ −Heat diffusivity (C_G) is measured in J/m²×K × $s^{1/2}$ using standard tables.
The overall surface area of the mould channel in contact with fluid is 1680*$10^{(-6)}$ m², assuming increased heat loss along the channel surfaces.

Journal of Information Systems Engineering and Management
2025, 10(4)
e-ISSN: 2468-4376
https://www.jisem-journal.com/

Research Article

Table **11** presents the total surface area of valve body casting mould channels and the parts that only interacted with fluid flow during mould cavity filling from the sprue entrance to the ingate section.
L_A denotes the lateral area, used in the valve body casting. Consequently, the loss is ascertained as

$$T_L = \frac{1680 * 10^{-6} * (1350 - 30) * \sqrt{9} * 3.21 * 10^3}{10.5 * 554} = 3.6\ ℃$$

Journal of Information Systems Engineering and Management
2025, 10(4)
e-ISSN: 2468-4376
https://www.jisem-journal.com/

Research Article

Table 11 Mould channel surface area in the fluid-filled contract

Sr. No.	Channel	Area in contact	Unit
1	Sprue	L_A=38.87*10^{-4}	m^2
2	Ingate	L_A=22.07*10^{-4}	m^2
Total		$16.80 * 10^{-4}$	m^2

The temperature reduction in the gating system channels is 3.6 °C, resulting in hot metal arriving to the ingate output cavity at a temperature of around 1346.4 °C.

3.2.19 Procedure for the solidification of the valve body casting

While flowing into the mould, liquid metal becomes solid metal. This is a very important step in the casting life cycle. The action can take seconds to hours, depending on the casting technique and size. The microstructure and mechanical and physical characteristics of the casting depend on the metal composition, solidification, and solid-state treatment [47].
The technique was first built using directed solidification, which guides metal from the mould cavity extremity to the riser. The mould has vent holes to release fuel bubbles, which cause valve body porosity. After creating the mould, it is positioned at a 90° angle to the horizontal stage to flow metal via the developed gating system to fill all voids. Heat transport methods including conduction and convection harden molten metal.

3.3 Process parameter selection

Control factors greatly impact valve body component rejection percentage. The requirements were defined and maintained following conversations with foundry managers, casters, mould producers, and pattern designers. Ambient operational conditions affect noise.
The study shows that 70% of casting rejections are due to moulding sand, 20% to pouring metal, and 10% to melting, pattern shop, and core. [48]
This prompted this investigation to focus on sand and molten metal. Mould shifts, swells, blow holes, shrinkage, and hot tears might arise from improper process parameter selection.
Since they determine ductile iron casting development, the analysed factors affect solidification rate directly and indirectly. The Ishikawa diagram revealed the most important and quantitative traits.

3.3.1 Ishikawa diagram

A Ishikawa diagram is a technique used for detecting the fundamental reasons for quality issues.[49] Ishikawa diagrams reveal the process factors that affect valve body quality during manufacture. The figure in Figure 2 was constructed. Mould, metal, sand, shake-out, and machine parameters are provided. Process parameters fall into five categories.

Based on literature review, and research gap the following criteria were chosen to demonstrate how variables affect valve body sand casting faults. The parameters include moisture (4.0%-6.0%), sand strength Kg/m² (10,000-14,000), AFS (40-60), and pouring temperature (1300-1400°C).

3.4 Formulating an experiment

Factors, interactions, and levels must be identified to design an experiment. Taguchi suggests two to five layers. This strategy organizes the experiment using orthogonal array column assignments. The number of components, their levels, and specified interactions define orthogonality. The research used three-level orthogonal arrays, with L9 (3^3) and L27 (3^7) being the most common possibilities for factors. We conclude that L9 is optimum for analysing three items at three levels. Minitab 18 was used to analyse valve body data from a foundry production system. The process's most influential parameter was also found.

3.4.1 Level selection and experimental variables

Mould hardness, AFS number, sand strength, and moisture content are process parameters in this study. Control factors in this process may affect valve body product quality. Three levels were used to analyse each control component. After interviewing production workers and reviewing the foundry's valve body manufacturing process's most typical settings, factor values were determined. (

Journal of Information Systems Engineering and Management
2025, 10(4)
e-ISSN: 2468-4376
https://www.jisem-journal.com/

Research Article

Table 12 and

Trial number	Moisture content (%)	AFS number	sand strength (Kg/cm²)	Pouring temperature ℃
1.	4	40	10000	1300
2.	4	50	12000	1350
3.	4	60	14000	1400
4.	5	40	12000	1300
5.	5	50	14000	1350
6.	5	60	10000	1400
7.	6	40	14000	1300
8.	6	50	10000	1350
9.	6	60	12000	1400

).

Table 12 Factors and configuration

Sr. No.	Parameter	Designation	Small level 1	Middle level 2	Elevated level 3
1.	Moisture content (%)	P	4	5	6
2.	AFS Number	Q	40	50	60
3.	Sand strength Kg/cm²	R	10000	12000	14000
4.	Pouring temperature ℃	S	1300	1350	1400

Table 13 Three variables and three states make up the field in the orthogonal array.

Trial number	Moisture content (%)	AFS number	sand strength (Kg/cm²)	Pouring temperature ℃
10.	4	40	10000	1300
11.	4	50	12000	1350
12.	4	60	14000	1400
13.	5	40	12000	1300
14.	5	50	14000	1350
15.	5	60	10000	1400
16.	6	40	14000	1300
17.	6	50	10000	1350
18.	6	60	12000	1400

3.4.2 Choosing an orthogonal grid

More than two levels of sand-casting parameters are needed to discover non-linear interactions. Levels for each control parameter define the experimental domain. Three levels are assigned to each control component. Since noise sensitivity generally stays constant with slight control factor modifications, levels must be selected. Selecting a large experimental domain helps identify control parameter favourable and unfavourable locations. The choice of Orthogonal array is contingent upon the following factors:

(i) The quantity of elements and interactions of significance

(ii) The quantity of levels for each component of interest

These two criteria determine the experiment's total degrees of freedom. Each component has degrees of freedom equal to levels minus one. Assuming no interactions, the factors' DOF are:

$DOF = 1 + (@of\ factors) * (@of\ levels - 1)$ ... (18)

Where DOF is total degree of freedom.

$$DOF = 1 + \big(4 * (3 - 1)\big) = 9$$

The system degree of freedom (D_A) in an OA can be calculated as shown in equation 19, where n is number of experiment run or trial done.

Journal of Information Systems Engineering and Management
2025, 10(4)
e-ISSN: 2468-4376
https://www.jisem-journal.com/

Research Article

$D_A = n - 1$ ... (19)

$$D_A = 9 - 1 = 8$$

To pick the specific orthogonal array for an experiment, the following inequality must be fulfilled.

$$DOF \leq D_A$$

The product's total DOF is less than or equal to its system D_A. Orthogonal arrays (OA) are feasible.

3.4.3 Performing an investigation

Using Minitab 18, a statistical program, experimental examination of valve body products has been carried out based on the collected data. Depending on the number of parameters impacting product quality, L9 (3^3) orthogonal arrays have been used for valve body manufacture. Below you can see the complete experiment and a summary of the findings.

3.5 Simulation of the casting process

ProCAST helps the industry create novel casting processes, optimize current ones, solve problems, and design dies. ProCAST program simulated the casting process's succeeding steps. The ProCAST receives a SolidWorks geometric model, as shown in Figure 8. 3D modelled geometry was saved in IGES format and loaded into ProCAST. Initial 3D model repair and assembly occurred inside the visible mesh. CAD design changes may be needed if complications develop. A 2D surface mesh was produced by selecting the edge group element size and validated as suitable. Additionally, a 3D volume mesh was produced. Input parameters in the software were, the volume manager's moulding material and alloy element are silica sand and ductile iron, with starting working temperatures of 30 °C and 1350 °C. The interface manager chose according to h = 1000W/m2/k. Inlet mass flow rate as 185 kg/s was taken as input data. The simulation process settings use gravity casting and activate the heat model, porosity model, and TH-Module. Selecting 4 cores started simulation. After successful execution, the casting simulation software produces graphical and video data that are evaluated to predict flaws. Figure 9 shows the valve body mesh shape and gating mechanism.

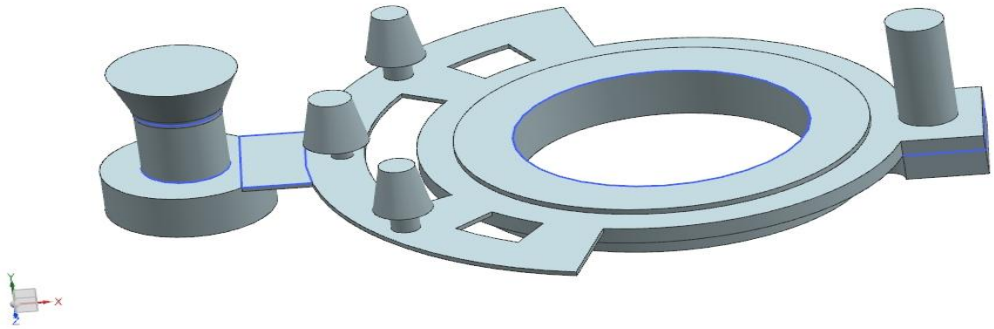

Figure 11 Proposed 3D CAD model of valve body

Journal of Information Systems Engineering and Management
2025, 10(4)
e-ISSN: 2468-4376
https://www.jisem-journal.com/

Research Article

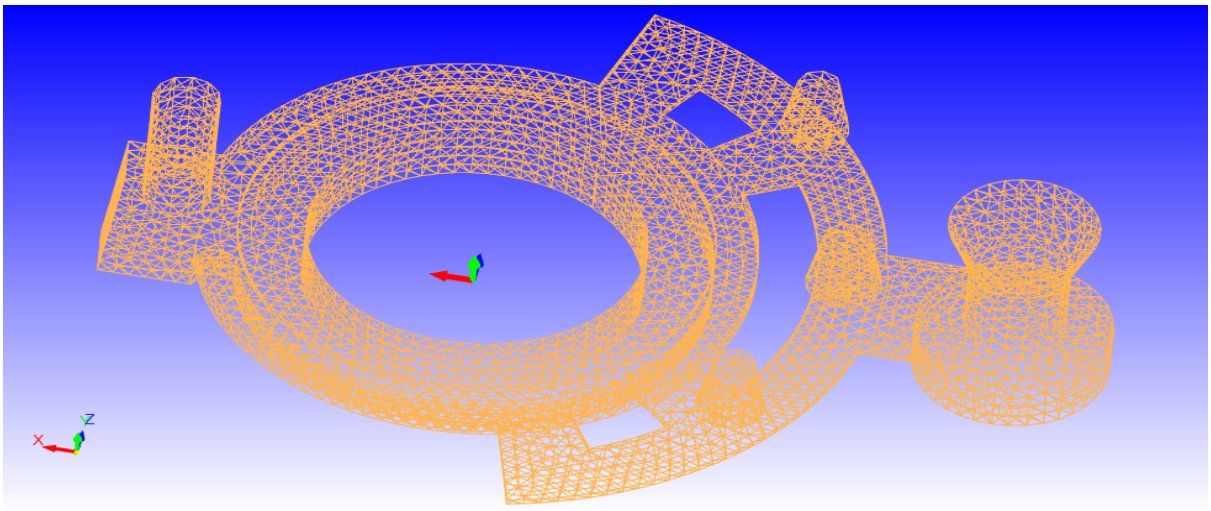

Figure 12 3D geometry of meshed valve body

3.6 Analysis of casting simulation

ProCAST models valve body sand casting fluid dynamics and solidification. To predict molten metal solidification in the mould, casting simulation and analysis were done.

3.6.1 Analysis of the filling process

The fill time is the time needed to fill a component section with liquid metal. Tapered sprue and pressured gating system design transfer molten metal through valve body's gating system. The gate lets molten metal enter the mould and rise relatively evenly until it fills the hollow. Figure 16 shows how metal infill in the mould cavity allows liquid metal to flow smoothly while preventing cold metal from entering. Ductile iron pours at 1350 °C. Complete mould cavity filling should take 9 seconds. The simulation results show that mould cavity was occupied efficiently and consistently exclusive of disorder or temperature changes. Without gasses, slags, inclusions, dross, or other impurities, the colour distribution is uniform. This shows a good casting simulation result as the riser was recently filled to address valve body casting shrinkage.

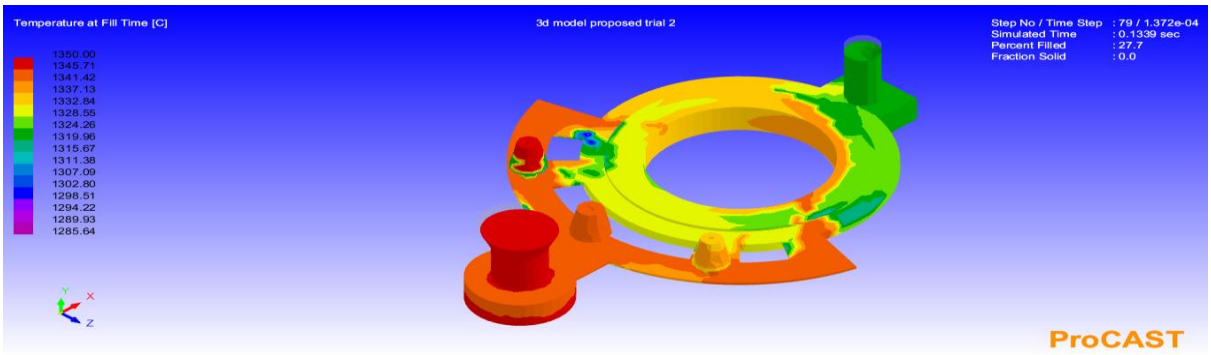

Figure 13 Temperature at fill time

3.6.2 Analysis of Solidification Duration

Solidification time is the number of seconds needed for each valve body piece to solidify. This process lasts from pouring until solidification. Solidification time depends on volume-to-surface area ratio [52]. Valve body solidification begins when liquid metal enters the mould cavity. Complex physical, thermal, and metallurgical processes occur during valve body casting solidification. Directional solidification is necessary for valve body casting. The thinnest portion is solidified first, followed by the thickest and riser. Heat transmission from the casting to the outside causes solidification. Heat from the casting's inside must travel several paths. At 1236 °C, metal solidifies. Metal solidification ends at 1131 °C solidus.

Directional solidification time charts for valve body casting are shown in Figure 11. This information helps detect isolated molten metal patches in the casting and offers a valve body-wide perspective of directional

solidification. The graphical findings show solidification time throughout time steps in various colours. Thus, the model has no volumetric shrinkage problems.

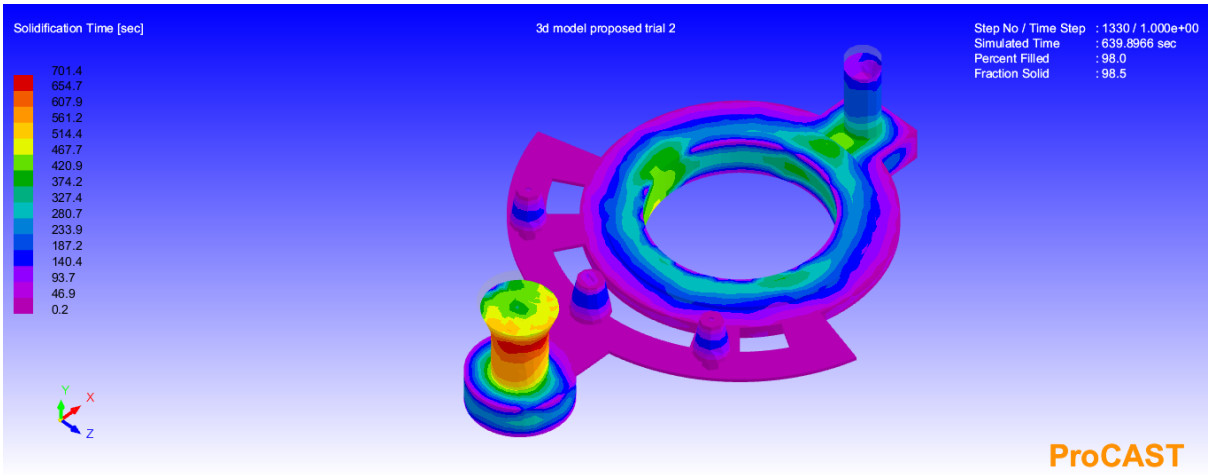

Figure 14 solidification time

3.6.3 Analysis of solid fraction time

An essential part A piece of the valve body casting takes minutes to reach the crucial fraction solid threshold. After pouring, molten metal stops flowing as liquid feed metal. The mushy zone's solid-liquid metal ratio changes with time and temperature. The solidification process ends when the last drop of liquid metal solidifies.[53]

The valve body and gating mechanism maintain the same temperature range throughout mould filling. Simulations show directed solidification in valve body casting. As latent heat is released, liquid metal in the mould cavity solidifies. Figure 12 depicts fraction solidification. All-white model indicates solid valve body.

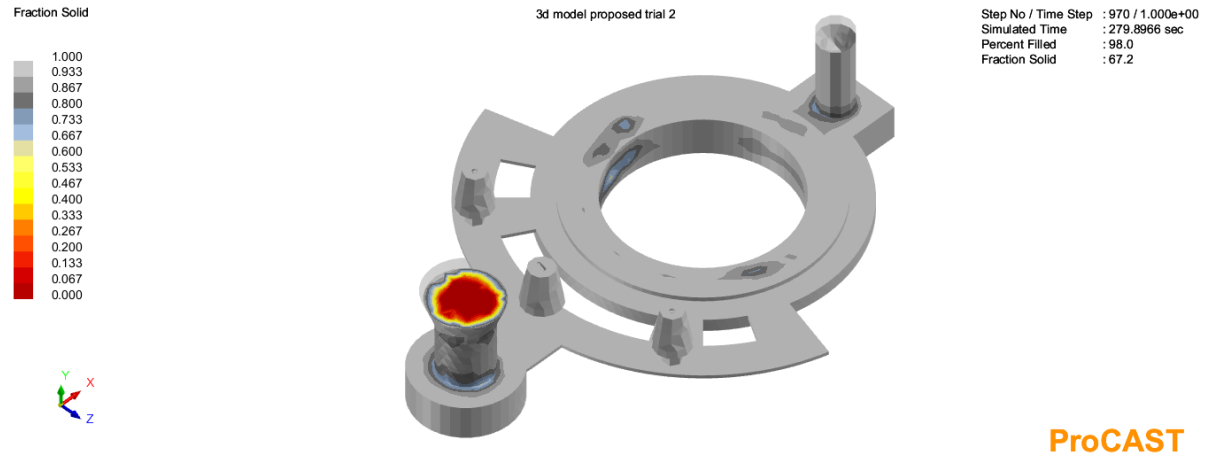

Figure 15 Fraction of solid

3.6.4 Analysis of shrinkage porosity

Cavities in components may weaken material due to shrinkage porosity flaws. Surface flaws may reduce aesthetics and corrosion resistance. As materials solidify, shrinkage porosity develops from mould filling to final solidification. Material shrinking causes porosity.

Computer models of filling and solidification predict shrinkage porosity. When heat is released, liquid metal solidifies. The valve body casting procedure has caused shrinkage porosity.

Figure 13 shows shrinkage porosity in casting component simulations. Riser and valve body components feature shrinkage porosities. Improving the component's shrinkage porosity in the simulation involves strategically situating the gate and riser and adding feeders.

Journal of Information Systems Engineering and Management
2025, 10(4)
e-ISSN: 2468-4376
https://www.jisem-journal.com/

Research Article

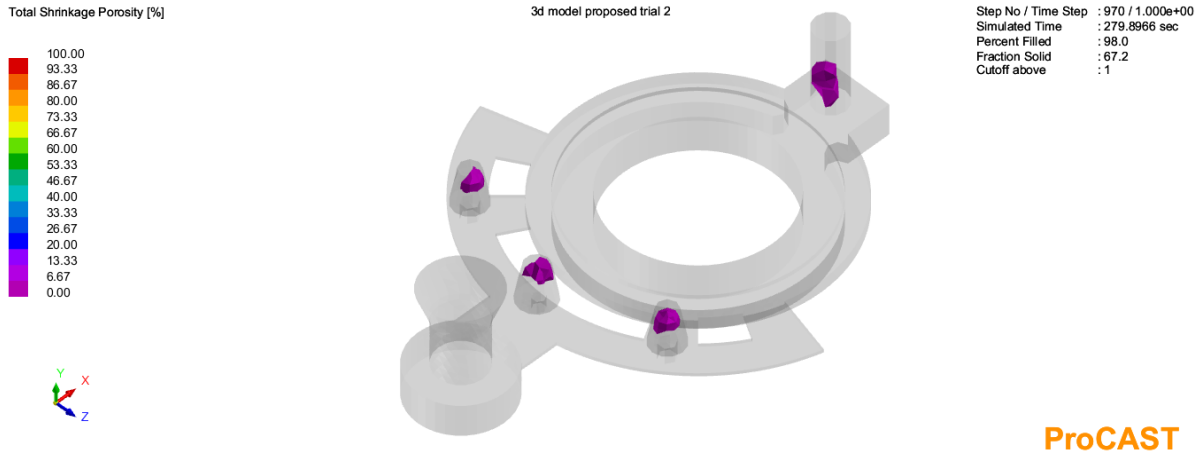

Figure 16 Shrinkage porosity

4Result and discussion

A case study was done on a ductile iron valve body with a 380-mm outside diameter, 200-mm inner diameter, and 45-mm height. NX 10.0 program creates valve body casting model pieces. All these components are then placed in the mould according to their places.

4.1 Findings and analysis from the experiment

The signal-to-noise ratio formulae depend on the response variables: nominal is best, smaller values are better, and larger values are better. Fewer casting flaws mean better process performance.
The repetition strategy adopted was the single repetition randomization. It used the same parameters for the repeated numerical experiments. From the company's data sheet, the percentage of defect was obtained for each repetition and each trial condition. We computed the defect percentage of each iteration from the equation (20).

$$\%\ of\ defects = \frac{Number\ of\ defects\ arrising\ from\ molding\ process}{Total\ numbers\ of\ flaws\ occuring\ in\ the\ process} \quad (20)$$

Nine experiments with two replicates of each factor level are included in Table 14.

Table 14 Trials executed throughout nine experiments with two replications

Experiment No.	P	Q	R	S	Run 1	Run 2
1.	4	40	10000	1300	7	6.4
2.	4	50	12000	1350	5.7	5.4
3.	4	60	14000	1400	6.5	6.4
4.	5	40	12000	1300	6.8	8.3
5.	5	50	14000	1350	4.3	4.2
6.	5	60	10000	1400	5.6	5.3
7.	6	40	14000	1300	4.5	3.9
8.	6	50	10000	1350	4.1	5.2
9.	6	60	12000	1400	3.9	4.3

Table 15 shows experimental valve body quality process factor predictions. A "smaller is better" quality trait describes casting flaws. The S/N ratio and casting defect average were computed for each experimental condition.
The mean and S/N ratio for each experiment can be calculated by using Equations (21) and (22) respectively.

$$Mean = \frac{Aggregate\ of\ individual\ trials\ from\ each\ experiment}{N} \quad \ldots (21)$$

$$\frac{S}{N} ratio = -10log\left(\frac{1}{n}\sum_{i=1}^{n} Y_i^2\right) \quad \ldots (22)$$

The S/N ratio measures noise sensitivity. The variable n indicates the number of orthogonal array tests, whereas Y_i^2 holds the ith measured value. *Table 15* shows each experiment's mean and signal-to-noise ratios.
Table 15 Mean and S/N ratio of the experimental trials are presented for analysis.

Journal of Information Systems Engineering and Management
2025, 10(4)
e-ISSN: 2468-4376
https://www.jisem-journal.com/

Research Article

Experiment No.	P	Q	R	S	Run 1	Run 2	Mean	S/N ratio
1.	4	40	10000	1300	7	6.4	6.7	-16.5215
2.	4	50	12000	1350	5.7	5.4	5.55	-14.8859
3.	4	60	14000	1400	6.5	6.4	6.45	-16.1912
4.	5	40	12000	1300	6.8	8.3	7.55	-17.5589
5.	5	50	14000	1350	4.3	4.2	4.25	-12.5678
6.	5	60	10000	1400	5.6	5.3	5.45	-14.7279
7.	6	40	14000	1300	4.5	3.9	4.2	-12.4650
8.	6	50	10000	1350	4.1	5.2	4.65	-13.3491
9.	6	60	12000	1400	3.9	4.3	4.1	-12.2557

4.1.1 Signal-to-noise ratio analysis

The "signal-to-noise" ratio is the most important robustness indicator in factor design. According to the Taguchi technique, "signal" refers to a desirable target (more castings authorised) and "noise" refers to an undesirable quantity.

According to *Table 16*, the S/N ratio values of distribution in every trial varied between –12.2557 (9th row) and -17.5589 (4th row). From each trial S/N ratio, the mean value of S/N for each component and level was obtained using Equation (22).

Table 16 S/N ratio findings of each experiment done

Experiment No.	P	Q	R	S	Run 1	Run 2	Mean	S/N ratio
1.	4	40	10000	1300	7	6.4	6.7	-16.5215
2.	4	50	12000	1350	5.7	5.4	5.55	-14.8859
3.	4	60	14000	1400	6.5	6.4	6.45	-16.1912
4.	5	40	12000	1300	6.8	8.3	7.55	-17.5589
5.	5	50	14000	1350	4.3	4.2	4.25	-12.5678
6.	5	60	10000	1400	5.6	5.3	5.45	-14.7279
7.	6	40	14000	1300	4.5	3.9	4.2	-12.4650
8.	6	50	10000	1350	4.1	5.2	4.65	-13.3491
9.	6	60	12000	1400	3.9	4.3	4.1	-12.2557

$SN_B = \frac{(S_{N1}+S_{N2}+S_{N3})}{3}$ .. (23)

The range (Δ) for each component was calculated by deducting the smallest value from the largest value within that factor after determining the average signal-to-noise (S/N) ratio. Table 17 shows the ranks based on each factor's range. S/N response Table 17shows that moisture content and pouring temperature affect product valve body casting output reaction the greatest, while sand strength has the least effect.

Table 17 Impact of each component on the response variable

Level	Moisture content	AFS number	Sand strength	Pouring temperature
1	-15.87	-15.52	-14.87	-13.78
2	-14.95	-13.60	-14.90	-14.03
3	-12.69	-14.39	-13.74	-15.70
Delta	3.18	1.91	1.16	1.92
Rank	1	3	4	2

4.1.2 Primary effect diagram for signal-to-noise ratios

The mean line of the S/N was used to predict the effect of each factor using Minitab software.Figure 17 shows that sand mould moisture and pouring temperature reduce casting flaws greatest, while sand strength has little effect.

Journal of Information Systems Engineering and Management
2025, 10(4)
e-ISSN: 2468-4376
https://www.jisem-journal.com/

Research Article

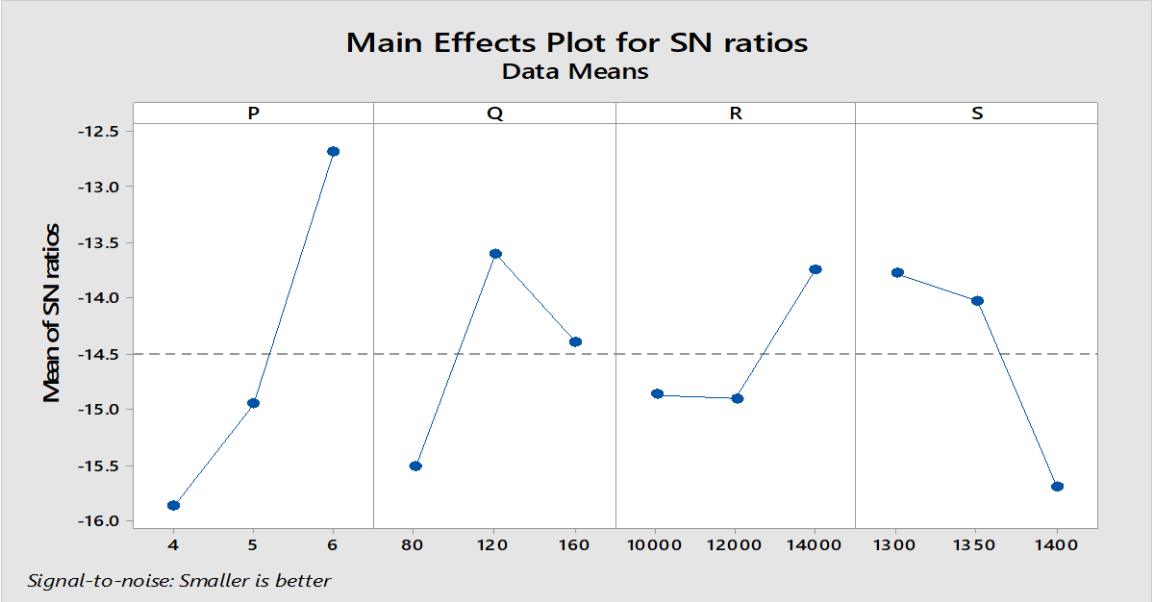

Figure 17 Main effects plot for S/N ratio

4.1.3 Analysis of variance

ANOVA was used to find the control factor that significantly affects quality. ANOVA calculates component significance based on their proportion contribution to valve body casting response.
Data is analysed using ANOVA after experiments. The essential factors, their relationships, and casting fault-affecting parameters have been identified in several testing setups. Table 18 shows analysis of variance among the three parameters viz. moisture content, AFS number and sand strength.
Based on experimental method, moisture content considerably impacts S/N ratio (Table 17).

Table 18 Analysis of Variance

Source	DF	Seq SS	Contribution	Adj SS	Adj MS	F-Value	P-Value
moisture content	2	5.962	47.90%	5.962	2.9808	2.16	0.317
AFS number	2	2.712	21.79%	2.712	1.3558	0.98	0.505
sand strength	2	1.007	8.09%	1.007	0.5033	0.36	0.733
Error	2	2.765	22.22%	2.765	1.3825		
Total	8	12.445	100.00%				

4.1.4 Pooling of error

Pooling pools together column effects to make error variance estimation. Pooling estimates of column impact for comparing if smallest column is different from one of the higher values. Significant F-ratio using an F-test, merging two effects unless one finds it that produces significant F-ratio. Pooling could result in having more pertinent columns to accept the experiment and conclude the right effect.
Since the contribution % and F-ratio for moisture content was small, they merged with error estimates of degrees of freedom, sums of squares and variance to reformulate the table after pooling approach. (Table 19).
The factors are aggregated to derive new S_e and F_e:
Sum of squares of error:

$S_e = S_T - (S_P + S_Q + S_R)$ ... (24)

$$S_e = 12.4450 - (5.962 + 2.712 + 1.007) = 2.765$$

Degree of freedom of error term:

$f_e = f_T - (f_P + f_Q + f_R)$ ... (25)

$$f_e = 8 - (2 + 2 + 2) = 2$$

Variances of error calculate as:

$V_e = \frac{S_e}{f_e}$ ... (26)

$$V_e = \frac{2.765}{2} = 1.3825$$

Journal of Information Systems Engineering and Management
2025, 10(4)
e-ISSN: 2468-4376
https://www.jisem-journal.com/

Research Article

Table 19 Outcomes of the variance analysis following the combined error assessment

Source	DF	Seq SS	Contribution	Adj SS	Adj MS	F-Value	P-Value
moisture content	2	5.962	47.90%	5.962	2.9808	2.16	0.317
AFS number	2	2.712	21.79%	2.712	1.3558	0.98	0.505
sand strength	2	1.007	8.09%	1.007	0.5033	0.36	0.733
Pooled Error	2	2.765	22.22%	2.765	1.3825		
Total	8	12.445	100.00%				

4.2 Analysis of raw data from investigational outcomes

Table 19 shows the average casting fault percentage and S/N ratio for each parameter at different levels. Thus,

Table **20** shows that the percentage of defects is lowest, and the S/N ratios are highest for the second moisture content (P2), third AFS (Q3), second sand strength (R2), and second pouring temperature (S2).

Table 20Mean values of casting imperfections and signal-to-noise ratios

Factors	Level 1		Level 2		Level 3	
	Casting defects	S/N ratio	Casting defects	S/N ratio	Casting defects	S/N ratio
P	4.232	-12.5309	3.32	-10.4227	5.65	-15.0409
Q	6.23	-15.8897	5.23	-14.3700	3.56	-11.0289
R	3.823	-11.6480	2.85	-9.0968	4.0	-12.0411
S	5.52	-14.8387	3.73	-11.4341	4.5	-13.0642

4.3 Validation of experimental findings

The confirmation run ensured that the control parameter settings will provide better results than in the original experiment. The confirmation experiments verify that an experiment's components and levels affect a product or process's behaviour. A confirmation result averaging within confidence bounds implies that the relevant components and their amounts were correctly chosen to obtain the intended results. If the mean of the confirmation experiment results falls outside the confidence interval, the parameters and/or control levels for reaching the intended value are either erroneous or entail excessive measurements, needing extra testing.[51] Three confirmation tests were conducted under Table 21's optimum process conditions. Respondents reported 1.25 % casting flaws in each trial, matching the confidence interval. Confirmation studies show that 1.25 is less than 10%, the maximum for ductile iron casting. The parameters and their amounts are vital to the desired result.

Table 21 Results of the confirmation experiment on valve body green sand casting

Experiment no.	% of defect		Average % of casting defect
	Trial 1	Trial 2	
1	1.3	1.2	1.25
2	1.1	1.4	1.25
Total average			1.25

This work uses Taguchi optimization to find the best parametric combination to reduce sand cast valve body flaws. Economic variables determine the percentage contribution and ideal parameters in Table 22. Three factors were used to experimentally determine process variable hierarchies affecting casting faults. A small number of experiments determined the appropriate valve body casting fault percentage. Valve body cast product is shown in Figure 8.

Journal of Information Systems Engineering and Management
2025, 10(4)
e-ISSN: 2468-4376
https://www.jisem-journal.com/

Research Article

Figure 18 Valve body casting

Table 22 Percentage contribution and optimal parameters considering economic factors

Factor	Parameter	S/N ratio of casting defect (%)	Optimum level	Optimum value
P	Moisture content (%)	47.90%	2	5
Q	AFS Number	21.79%	3	60
R	Sand strength Kg/cm²	8.09%	2	12000
S	Pouring temperature ℃	22.22%	2	1350

4.4 Simulation results

After doing simulation of existing gating design, and proposed gating design, following Figure 19 shows comparison of shrinkage and porosity results, from simulation results, in proposed gating design shows minor shrinkage across the gating components, and no evidence of shrinkages in valve body casting, and in existing shrinkage and porosity is exists in cast component itself and across gating components also.

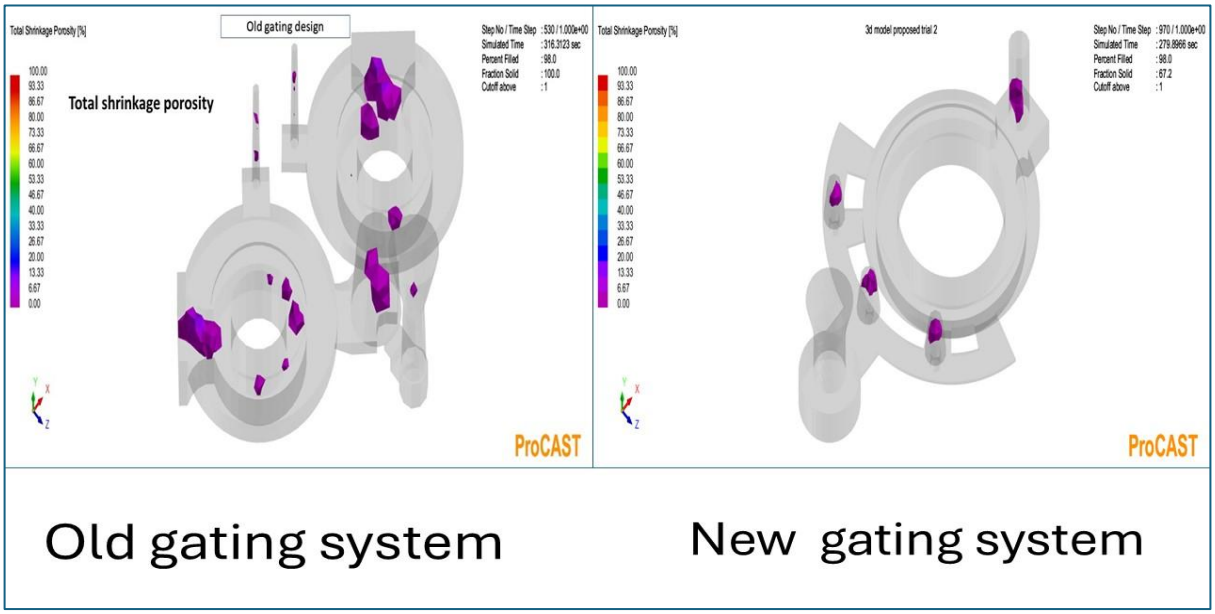

Figure 19 Comparison of simulation results

The following Figure 20 shows the comparison of simulation results of Niyama criterion, as per Niyama criterion for Ductile iron casting value should be greater than 70, and it is clear that in existing gating design the critical value of Niyam criterion is below 70 and in proposed gating design it is above the 70.

Journal of Information Systems Engineering and Management
2025, 10(4)
e-ISSN: 2468-4376
https://www.jisem-journal.com/

Research Article

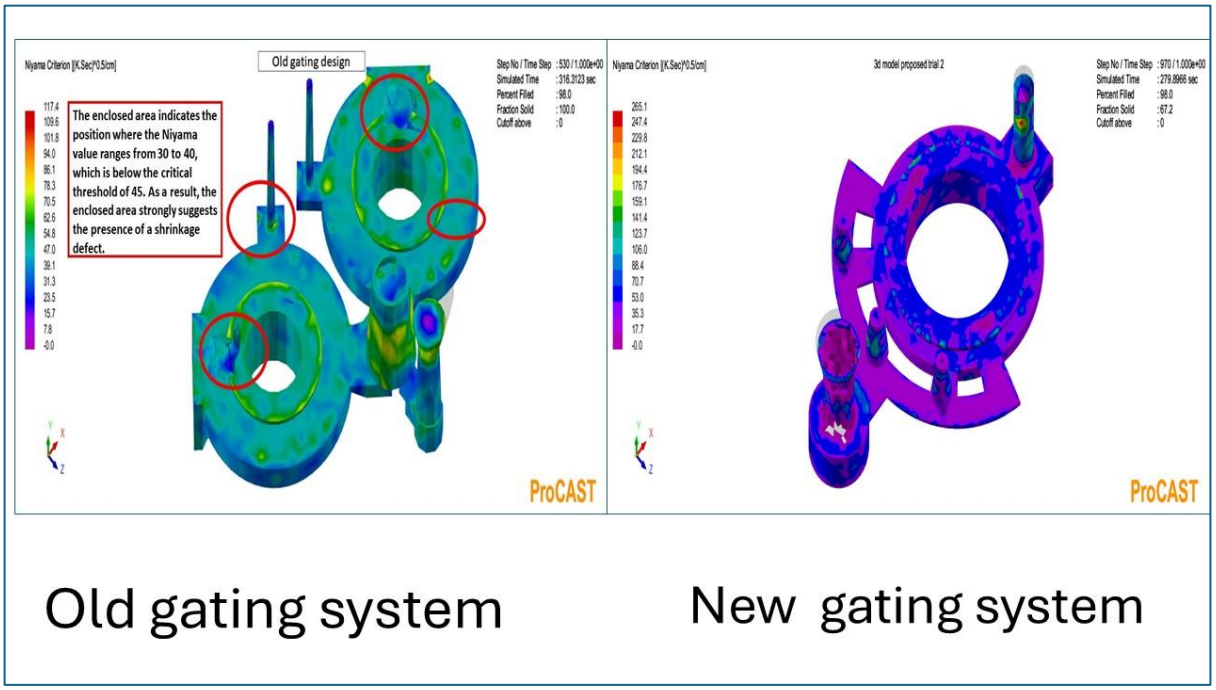

Figure 20 Comparison of Niyama Criterion

4.4.1 Experimental validation

Based on new gating system, experiment was carried out for three batch, each batch consisting of 200 valve body casting, and following result as shown in

Table 23, was obtained from the experiment, in which rejection due to shrinkage and porosity reduced to 1 % from 26 % earlier in the old gating design.

Table 23 Experiment for new gating design valve body casting

Batch No.	No. of valve body casted	No. of valve body rejected due to shrinkage defect	% rejection
1	200	3	1.5
2	200	2	1
3	200	1	0.5
Average rejection %			1

5 Conclusions

Statistical methods have been used to reduce sand cast valve body flaws. Table 18 shows that most factors affect casting fault mean and variance.
Conclusion from experiment and simulation study.

1.The implementation of Taguchi's method in the valve body sand casting process serves to:
- Improve quality and productivity of valve body casting
- Increase casting stability
- Higher yield is possible

2. Sand mould related defects were reduced from 9 % to 1.1 % and shrinkage defect reduced from 26 % to 1 %.

3. The experiment design determines optimal process parameters for the sand-casting valve body. Moisture (5%), pouring temperature (1350 °C), sand strength (12000 Kg/cm2), and AFS Number (60) are appropriate.
4. Percent contribution of each factor has been determined as follows:
moisture content 47.90%, pouring temperature at 22.22%, AFS Number at 21.79%, and sand strength at 8.09 % In addition, the percentage of improvement in the minimization of the casting defects of the valve body is at 90%.
5. Numerically, it's found that improper pattern usage within the gating system parts leads to misrun and volumetric shrinkage problems of valve body castings.
6. Casting simulation analysis evaluates these criteria: casting solidification time, filling, and mould geometry in the quality production of casting. To some extent, precise identification in the design time of these may assist in rendering effective casting solution in the reduction of valve body casting defects.
7. Experimental findings indicate that porosity problems in valve body castings and sintering in sand are caused by the lack of sintering strength in fine mixed moulding silica sand used in foundry processes.
8. Simulation adequately depicts filling and solidification while saving time, energy, labour, and financial resources (8). The valve body castings had volumetric solidification shrinkage and porosity issues, according to simulations.

Conflict of interest:
The authors have no conflict of interest.

Acknowledgments:
The researchers are grateful to Manager Mr. D.H.Patel of Fine Cast Foundry, India, for allowing us to perform the study. The researchers further thank Dr. S.K. Tareiya, Faculty, Government Polytechnic, Jamnagar, and Dr. Purvesh Nanavati, Assistant Professor, GEC, Gandhinagar, for their assistance, encouragement, and research facilities.

References

1. Chen, Z., et al., *Progress in numerical simulation of casting process*. Measurement and Control, 2022. **55**(5-6): p. 257-264.
2. You, L., et al., *Numerical simulation and casting process optimization of cast steel node*. The International Journal of Advanced Manufacturing Technology, 2023. **126**(11): p. 5215-5225.
3. Ambriško, Ľ. and L. Pešek, *Non-Contact Evaluation of Deformation Characteristics on Automotive Steel Sheets*. Metals, 2024. **14**(5): p. 566.
4. Jarfors, A., Q. Zhang, and S. Jonsson, *An a Priori Discussion of the Fill Front Stability in Semisolid Casting*. *Technologies 2022, 10, 67*. 2022, s Note: MDPI stays neutral with regard to jurisdictional claims in published ….
5. Ibraheem, A.M., *Ultra-clean steel production: Behavior of micro-sized alumina inclusions at the Ar gas/liquid steel interface*. 2023.
6. Malindžák, D., et al., *The methodology and model for in-process inventories calculation in the conditions of metallurgy production*. Metalurgija, 2015. **54**(1): p. 227-230.
7. Chakrabarti, A., *Casting technology and cast alloys*. 2022: PHI Learning Pvt. Ltd.
8. Mortazavi, P., *Large-scale experimental validation and design of resilient EBFs with cast steel replaceable modular yielding links*. 2023, University of Toronto (Canada).
9. Jolly, M. and L. Katgerman, *Modelling of defects in aluminium cast products*. Progress in Materials Science, 2022. **123**: p. 100824.
10. Gouttebroze, S., et al. *Modelling of major phases formation during solidification of Ferro-Silicon-Magnesium*. in *IOP Conference Series: Materials Science and Engineering*. 2023. IOP Publishing.
11. Alizadeh, M.H., M. Ajri, and V.A. Maleki, *Mechanical properties prediction of ductile iron with spherical graphite using multi-scale finite element model*. Physica Scripta, 2023. **98**(12): p. 125270.
12. Zor, M.M., et al., *Reducing casting defects in ductile iron castings by optimized pouring system*. Engineering Applications, 2023. **2**(1): p. 26-31.
13. Kugu, O.C. and O. Yetik, *Evaluation of flow simulation results of gray cast iron brake disk for alternative gating system design*. Journal of Thermal Analysis and Calorimetry, 2024: p. 1-19.
14. Kumar, R., et al., *Optimization and empirical studies of riser design in sand casting process using different mould properties*. International Journal on Interactive Design and Manufacturing (IJIDeM), 2024: p. 1-12.

15. Janakiraman, V., et al. *Enhancing Dimensional Geometry Casting using Computer Modeling*. in *E3S Web of Conferences*. 2024. EDP Sciences.
16. Angella, G., et al., *An Insight into the Defects-Driven Plasticity in Ductile Cast Irons*. Materials, 2023. **16**(10): p. 3748.
17. Liu, L., et al., *Numerical Simulation on Impeller Casting Defects and Optimization*. Mathematical Problems in Engineering, 2023. **2023**(1): p. 8884270.
18. Nam, J.-H., S.-M. Lee, and S.-H. Lee, *Guaranteed soundness of heavy section spheroidal graphite cast iron based on a reliable C and Si ranges design*. Metals and Materials International, 2023. **29**(8): p. 2151-2158.
19. Lacaze, J., J. Sertucha, and U. de la Torre, *Density change upon solidification of silicon cast irons*. International Journal of Metalcasting, 2023. **17**(3): p. 1493-1506.
20. Alonso, G., et al., *The effects of holding time in the heating/pouring unit on the metallurgical quality of spheroidal graphite iron*. International Journal of Metalcasting, 2023. **17**(2): p. 1361-1372.
21. Futas, P., et al., *Elimination of Shrinkage in Ductile Iron Castings Using Computer Simulation of Casting and Solidification*. Processes, 2024. **12**(3): p. 506.
22. Sangame, B.B. and Y.P. Reddy, *Investigation on effect of carbon equivalent and inoculation on the solidification and shrinkage tendency of ductile cast iron using thermal analysis*. Multidiscipline Modeling in Materials and Structures, 2024. **20**(1): p. 1-17.
23. Keskin, M.E., et al., *Investigation of The Effect of Moulding Material Difference on Design in GGG70 Ductile Cast Iron Production*. Türk Doğa ve Fen Dergisi, 2024. **13**(2): p. 14-20.
24. Baitiang, C., et al., *Data-driven process analysis for iron foundries with automatic sand moulding process*. International Journal of Metalcasting, 2024. **18**(2): p. 1135-1150.
25. Singh, D., *Design Considerations in Casting*, in *Fundamentals of Manufacturing Engineering: Concepts and Applications*. 2024, Springer. p. 169-188.
26. Shuvo, M.M., et al., *Toward Reducing Casting Defects via 3D Risers via 3D Sand-Printing: A Simulation Study*. International Journal of Metalcasting, 2024: p. 1-14.
27. Sabik, V., *THE NUMERICAL SIMULATION OF CASTING PROCESS OF CAST MADE FROM AUSTEMPERED DUCTILE IRON (ADI)*. International Multidisciplinary Scientific GeoConference: SGEM, 2023. **23**(2.1): p. 105-112.
28. Kumar, S., G. Mandal, and K. Mukherjee, *Stretch Flangeability of Low Carbon Micro-alloyed Ferrite-Pearlite and Ferrite-Bainite Steel*. Metallurgical and Materials Transactions A, 2024. **55**(10): p. 4093-4107.
29. Zhang, C., et al., *Effect of normalizing temperature on microstructure and mechanical properties of ductile iron for piano iron plate*. Metalurgija, 2025. **64**(1-2): p. 13-16.
30. Norouzian, M., M.A. Elahi, and P. Plapper, *A review: Suppression of the solidification cracks in the laser welding process by controlling the grain structure and chemical compositions*. Journal of Advanced Joining Processes, 2023. **7**: p. 100139.
31. Ibrahim, M., *An overview on Thin Wall Cast Iron Castings and its Applications in Automotive Industry*. International Journal of Materials Technology and Innovation, 2023. **3**(1): p. 57-69.
32. Gundlach, R. and J.M. Tartaglia, *Achieving Higher Strength and Ductility in Heavy-Section Ductile Iron Castings*. International Journal of Metalcasting, 2024: p. 1-26.
33. Khan, N.A., D. Chakraborty, and A. Kumar, *Optimization of Mechanical Properties for Spheroidal Graphite (SG) Iron Through Various Heat Treatment*. PROCESSING AND FABRICATION OF ADVANCED MATERIALS, VOLUME 1: Proceedings of the, 2024. **1**: p. 331.
34. Singh, J., et al. *Taguchi's based approach to optimize the foundry's green sand casting process parameters*. in *2024 3rd International Conference on Computational Modelling, Simulation and Optimization (ICCMSO)*. 2024. IEEE.
35. Ballance, O.J., *Sampling and randomisation in experimental and quasi-experimental CALL studies: Issues and recommendations for design, reporting, review, and interpretation*. ReCALL, 2024. **36**(1): p. 58-71.
36. Kumar, M. and J. Prakash, *Optimization of casting process parameters using Taguchi analysis*. Int. J. of Mech. Eng. and Res, 2015: p. 5-1.
37. Bekele, B.T., et al., *Simulation and experimental analysis of re-design the faulty position of the riser to minimize shrinkage porosity defect in sand cast sprocket gear*. Materials today: proceedings, 2022. **59**: p. 598-604.
38. Brown, J., *Foseco ferrous foundryman's handbook*. 2000: Butterworth-Heinemann.

Research Article

39. Muzakki, H., I. Millaily, and H. Winandar. *Gating System Measuring of Sandcasting*. in *IOP Conference Series: Materials Science and Engineering*. 2021. IOP Publishing.
40. Upadhyaya, R., et al., *Investigation of the Quality of Flywheel SG Iron Sand Casting Using the Optimized Riser Dimensions: Numerical Simulation and Experimental Validation*. International Journal of Metalcasting, 2024: p. 1-11.
41. Kim, Y.-C., et al., *Improvement of quality and yield for investment casting of centrifugal pump impeller by tilting mould and optimizing runner/riser system*. The International Journal of Advanced Manufacturing Technology, 2024. **130**(5): p. 2369-2379.
42. Gao, K. and Y. Peng, *Numerical simulation of fluid flow and free surface fluctuations during wheel and belt casting process*. Journal of Iron and Steel Research International, 2024. **31**(5): p. 1117-1126.
43. Ma, C., et al., *Flow field in slab continuous casting mould with large width optimized with high temperature quantitative measurement and numerical calculation*. Metals, 2021. **11**(2): p. 261.
44. Chelladurai, C., et al., *Analyzing the casting defects in small scale casting industry*. Materials Today: Proceedings, 2021. **37**: p. 386-394.
45. Hosseini, S.M. and E. Amani, *An improved combination of ruler and local electromagnetic brakes for continuous casting process*. Journal of Manufacturing Processes, 2023. **85**: p. 1037-1053.
46. Duarte, I.C.D., G.M.d. Almeida, and M. Cardoso, *Heat-loss cycle prediction in steelmaking plants through artificial neural network*. Journal of the Operational Research Society, 2022. **73**(2): p. 326-337.
47. Borsato, T., et al., *Long solidification time effect on solution strengthened ferritic ductile iron fatigue properties*. International Journal of Fatigue, 2021. **145**: p. 106137.
48. Kabnure, B.B., V.D. Shinde, and D.C. Patil, *Quality and yield improvement of ductile iron casting by simulation technique*. Materials Today: Proceedings, 2020. **27**: p. 111-116.
49. Chokkalingam, B., et al., *Investigation of shrinkage defect in castings by quantitative Ishikawa diagram*. Archives of Foundry Engineering, 2017.
50. Weldeanenia, K.G. and A.T. Abebe, *Optimization of sand casting process parameters for 46MnSi4 alloy steel trash plate castings applicable for valve body stand*. International Journal of Engineering Trends and Technology (IJETT), 2016. **41**(8).
51. Rajput, R., *A textbook of manufacturing technology: Manufacturing processes*. 2007: Firewall Media.
52. Wigger, T., et al., *In situ synchrotron investigation of degenerate graphite nodule evolution in ductile cast iron*. Acta Materialia, 2021. **221**: p. 117367.
53. Goodrich, G.M., et al., *Failures Related to Castings*, in *Analysis and Prevention of Component and Equipment Failures*. 2021, ASM International. p. 177-222.